AD_____

Award Number: DAMD17-00-1-0455

TITLE: Scanning Microwave Induced Acoustic Tomography

PRINCIPAL INVESTIGATOR: Lihong Wang, Ph.D.

CONTRACTING ORGANIZATION: Texas Engineering Experiment Station
College Station, Texas 77843-3000

REPORT DATE: October 2001

TYPE OF REPORT: Annual

PREPARED FOR: U.S. Army Medical Research and Materiel Command
Fort Detrick, Maryland 21702-5012

DISTRIBUTION STATEMENT: Approved for Public Release;
Distribution Unlimited

REPORT DOCUMENTATION PAGE

Form Approved
OMB No. 074-0188

1. AGENCY USE ONLY (Leave blank)	2. REPORT DATE	3. REPORT TYPE AND DATES COVERED
	October 2001	Annual (1 Oct 00 - 30 Sep 01)

4. TITLE AND SUBTITLE
Scanning Microwave Induced Acoustic Tomography

5. FUNDING NUMBERS
DAMD17-00-1-0455

6. AUTHOR(S)
Lihong Wang, Ph.D.

7. PERFORMING ORGANIZATION NAME(S) AND ADDRESS(ES)
Texas Engineering Experiment Station
College Station, Texas 77843-3000

E-Mail: LWang@tamu.edu

8. PERFORMING ORGANIZATION REPORT NUMBER

9. SPONSORING / MONITORING AGENCY NAME(S) AND ADDRESS(ES)
U.S. Army Medical Research and Materiel Command
Fort Detrick, Maryland 21702-5012

10. SPONSORING / MONITORING AGENCY REPORT NUMBER

11. SUPPLEMENTARY NOTES

12a. DISTRIBUTION / AVAILABILITY STATEMENT
Approved for Public Release; Distribution Unlimited

12b. DISTRIBUTION CODE

13. ABSTRACT *(Maximum 200 Words)*

Since the grant was awarded in October 2000, we have published three peer-reviewed journal articles, published one conference proceedings article, delivered 16 invited talks, and graduated one M.S. student. This research has been successful and rewarding. We are well prepared to continue the project with greater successes.

Until cancer is eradicated by preventative measures, the grand challenge in cancer research is early-cancer detection because the cure rate of cancers is much improved if they are detected early. Cancerous breast tissues are found to be 2–5 times more strongly absorbing than surrounding normal breast tissues in the microwave, which has been attributed to an increase in bound water and sodium within malignant cells. The combination of ultrasound and microwave has provided us a unique opportunity for early-cancer imaging with high resolution and high contrast. We have made significant technical progress in thermoacoustic imaging including imaging configuration, data processing, and reconstruction. We have successfully imaged biological tissue with high resolution and high contrast. We look forward to meeting this grand challenge.

14. SUBJECT TERMS
Detection, photoacoustic effect, microwave, ultrasonography

15. NUMBER OF PAGES
30

16. PRICE CODE

17. SECURITY CLASSIFICATION OF REPORT	18. SECURITY CLASSIFICATION OF THIS PAGE	19. SECURITY CLASSIFICATION OF ABSTRACT	20. LIMITATION OF ABSTRACT
Unclassified	Unclassified	Unclassified	Unlimited

Table of Contents

Introduction

A novel imaging technology, scanning microwave-induced-acoustic tomography, will be developed for breast imaging. X-ray mammography and ultrasonography are the current clinical tools for breast-cancer screening and detection. Mammography is the "gold standard", however, uses ionizing radiation and has difficulties imaging pre-menopausal breasts, which are radiographically dense. Ultrasonography is an adjunct tool to x-ray mammography and cannot detect many of the nonpalpable tumors. The cure rate of breast cancers is improved if they are detected early. To provide a new non-invasive, non-ionizing diagnostic tool for detection of early breast cancers, we will develop real-time microwave-induced-acoustic tomography for breast imaging. Microwave-induced-acoustic tomography is based on the photoacoustic effect, generation of acoustic wave by deposition of short-pulse electromagnetic energy safely into biological tissues. The microwave for this technology is short-pulsed, and its power is within the IEEE safety limits. The microwave-induced acoustic wave is then detected with an ultrasonic detector for imaging. The contrast between tumors and normal tissues in the microwave regime is significantly better than other imaging modalities. Cancerous breast tissues are found to be 2-5 times more strongly absorbing than surrounding normal breast tissues in the microwave, which has been attributed to an increase in bound water and sodium within malignant cells. However, pure-microwave imaging is fundamentally limited to poor resolution (on the order of 10 mm) because of the large wavelength of microwave. Ultrasonic imaging has good resolution (on the order of 1 mm) but has a poor contrast between tumors and normal tissues. Microwave-induced-acoustic tomography combines the contrast advantage of purely-microwave imaging and the resolution advantage of purely-ultrasonic imaging, therefore, has the potential for detection of early breast cancers and for assessing and monitoring treatments as well.

Body

Paper 1

Y. Xu and L.-H. Wang, "Signal processing in scanning thermoacoustic tomography in biological tissues," Medical Physics 28 (7), 1519–1524 (2001).

See Appendix 1 for the full article.

Microwave-induced thermoacoustic tomography was explored to image biological tissues. Short microwave pulses irradiated tissues to generate acoustic waves by thermoelastic expansion. The microwave-induced thermoacoustic waves were detected with a focused ultrasonic transducer to obtain two-dimensional tomographic images of biological tissues. The dependence of the axial and the lateral resolutions on the spectra of the signals was studied. A reshaping filter was applied to the temporal piezoelectric signals from the transducer to increase the weight of the high-frequency components, which improved the lateral resolution, and to broaden the spectrum of the signal, which enhanced the axial resolution. A numerical simulation validated our signal-processing approach.

Paper 2

M. Xu, G. Ku, and L.-H. Wang, "Microwave-induced thermoacoustic tomography using multi-sector scanning," Medical Physics 28 (9), 1958–1963 (2001).

See Appendix 2 for the full article.

A study of microwave-induced thermoacoustic tomography of inhomogeneous tissues using multi-sector scanning is presented. A short-pulsed microwave beam is used to irradiate the tissue samples. The microwave absorption excites time-resolved acoustic waves by thermoelastic expansion. The amplitudes of the acoustic waves are strongly related to locally absorbed microwave-energy density. The acoustic waves may propagate in all spatial directions. A focused ultrasonic transducer is employed to acquire temporal acoustic signals from multiple directions. Each detected signal is converted into a one-dimensional (1-D) image along the acoustic axis of the transducer. The cross-sectional images of the tissue samples are calculated by combining all of the 1-D images acquired in the same planes.

Paper 3

D. Feng, Y. Xu, G. Ku, and L.-H. Wang, "Microwave-induced thermoacoustic tomography: reconstruction by synthetic aperture," Medical Physics 28 (12), 2427–2431 (2001).

See Appendix 3 for the full article.

We have applied the synthetic-aperture method to linear-scanning microwave-induced thermoacoustic tomography in biological tissues. A non-focused ultrasonic transducer was used to receive thermoacoustic signals, to which the delay-and-sum algorithm was applied for image reconstruction. We greatly improved the lateral resolution of images and acquired a clear view of the circular boundaries of buried cylindrical objects, which could not be obtained in conventional linear-scanning microwave-induced thermoacoustic tomography based on focused transducers. Two microwave sources, which had frequencies of 9 GHz and 3 GHz, respectively, were used in the experiments for comparison. The 3-GHz system had a much larger imaging depth but a lower signal-noise ratio than the 9-GHz system in near-surface imaging.

Paper 4

M. Xu, X. Wang, and L.-H. Wang, "High-resolution thermoacoustic tomography of biological tissue," in Biomedical Optoacoustics III, A. A. Oraevsky, ed., Proc. Soc. Photo-Opt. Instrum. Eng. 4618, in press. San Jose, CA, Jan. 20–21, 2002.

See Appendix 4 for the full article.

A study of pulsed-microwave-induced thermoacoustic tomography in biological tissues is presented. A backprojection algorithm based on rigorous theory is used to reconstruct the cross-sectional image from the thermoacoustic measurement in a circular configuration that encloses the sample under study. The results demonstrate the possibility of application in detecting small

tumors buried in biological tissues using microwave absorption contrast and ultrasound spatial resolution. Finally, the method is compared with laser-induced thermoacoustic tomography.

Statement of Work

Task 1:Setting up the scanning microwave-induced-acoustic tomography (SMIAT) instrument, Months 1–12:

a. Modify/connect the microwave generator and the ultrasonic scanner.
b. Image biological tissues in vitro with SMIAT.

This task has been successfully accomplished as shown in the appended full articles. We are well prepared to continue the project.

Key Research Accomplishments

- A reshaping filter was applied to the temporal piezoelectric signals from the transducer to increase the weight of the high-frequency components, which improved the lateral resolution, and to broaden the spectrum of the signal, which enhanced the axial resolution.
- Microwave-induced thermoacoustic tomography of inhomogeneous tissues was implemented using multi-sector scanning. We solved the problem of blind surfaces using this approach.
- We have applied the synthetic-aperture method to linear-scanning microwave-induced thermoacoustic tomography in biological tissues for the first time.
- A backprojection algorithm based on rigorous theory was derived and was used to reconstruct the cross-sectional image from the thermoacoustic measurements in a circular configuration. The results demonstrate the possibility of application in detecting small tumors buried in biological tissues using microwave absorption contrast and ultrasound spatial resolution.

Reportable Outcomes

Peer-reviewed journal articles

1. Y. Xu and L.-H. Wang, "Signal processing in scanning thermoacoustic tomography in biological tissues," Medical Physics 28 (7), 1519–1524 (2001).

2. M. Xu, G. Ku, and L.-H. Wang, "Microwave-induced thermoacoustic tomography using multi-sector scanning," Medical Physics 28 (9), 1958–1963 (2001).

3. D. Feng, Y. Xu, G. Ku, and L.-H. Wang, "Microwave-induced thermoacoustic tomography: reconstruction by synthetic aperture," Medical Physics 28 (12), 2427–2431 (2001).

Conference presentations/proceedings

1. M. Xu, X. Wang, and L.-H. Wang, "High-resolution thermoacoustic tomography of biological tissue," in Biomedical Optoacoustics III, A. A. Oraevsky, ed., Proc. Soc. Photo-Opt. Instrum. Eng. 4618, in press. San Jose, CA, Jan. 20–21, 2002.

Invited talks

1. 12/13/2000, Ultrasound-mediated medical imaging: acousto-optical and thermo-acoustic tomographies. International Photonics Conference, Hsinchu, Taiwan.

2. 02/22/2001, Ultrasound-mediated medical imaging: acousto-optical tomography and thermo-acoustic tomography. Department of Bioengineering, University of Pennsylvania, Philadelphia, Pennsylvania.

3. 03/23/2001, Ultrasound-mediated medical imaging: acousto-optical tomography and thermo-acoustic tomography. Department of Bioengineering, University of Toledo, Toledo, Ohio.

4. 06/01/2001, Ultrasound-mediated biophotonic imaging: acousto-optical tomography and thermo-acoustic tomography. Institute of Laser Life Science, South China Normal University, Guangzhou, China.

5. 06/12/2001, Ultrasound-mediated biophotonic imaging: acousto-optical tomography and thermo-acoustic tomography. National Laboratory of Biomedical Photonics, Huazhong University of Science and Technology, Wuhan, China.

6. 06/21/2001, Ultrasound-mediated biophotonic imaging: acousto-optical tomography and thermo-acoustic tomography. Department of Biomedical Engineering, Shanghai Jiaotong University, Shanghai, China.

7. 08/17/2001, Ultrasound-mediated biophotonic imaging: acousto-optical tomography and thermo-acoustic tomography. School of Physical Sciences, University of Kent at Canterbury, UK.

8. 08/23/2001, Ultrasound-mediated biophotonic imaging: acousto-optical tomography and thermo-acoustic tomography. Gordon Research Conference on Photoacoustic and Photothermal Phenomena, Oxford, UK.

9. 08/24/2001, Ultrasound-mediated biophotonic imaging: acousto-optical tomography and thermo-acoustic tomography. Department of Medical Physics and Bioengineering, University College London, London, UK.

10. 08/28/2001, Ultrasound-mediated biophotonic imaging: acousto-optical tomography and thermo-acoustic tomography. Department of Physics, University of Texas at San Antonio, Texas.

11. 10/01/2001, Ultrasound-mediated biophotonic imaging: acousto-optical tomography and thermo-acoustic tomography. Department of Biological Systems Engineering, University of Nebraska—Lincoln, Lincoln, Nebraska.

12. 10/04/2001, Ultrasound-mediated biophotonic imaging. Invited *plenary* talk for Saratov Fall Meeting 2001—Workshop on Optical Technologies in Biophysics & Medicine, Saratov, Russia.

13. 10/25/2001, Ultrasound-mediated biophotonic imaging. Department of Physics, Texas A&M University, Texas.

14. 11/16/2001, Ultrasound-mediated biophotonic imaging. Program of Bioengineering, University of Houston, Houston, Texas.

15. 12/03/2001, Ultrasound-mediated biophotonic imaging. DOE/NIH Workshop on Applications of Thermography in Medical Diagnosis and Treatment, Bethesda, Maryland.

16. 01/25/2002, Ultrasound-mediated biophotonic imaging. Lawrence Livermore National Laboratory, Livermore, California.

Degrees

1. 09/1999–08/2001, Dazi Feng, Biomedical Engineering Program, Texas A&M University, College Station, Texas. Thesis title "Microwave-induced thermoacoustic tomography: reconstruction by synthetic aperture." Defended in 06/2001. M.S. degree conferred in 12/2001. Joined Nortel, Texas in 08/2001.

Conclusions

Since the grant was awarded in October 2000, we have published three peer-reviewed journal articles, published one conference proceedings article, delivered 16 invited talks, and graduated one M.S. student. This research has been successful and rewarding. We are well prepared to continue the project with greater successes.

Until cancer is eradicated by preventative measures, the grand challenge in cancer research is early-cancer detection because the cure rate of cancers is much improved if they are detected early. Cancerous breast tissues are found to be 2–5 times more strongly absorbing than surrounding normal breast tissues in the microwave, which has been attributed to an increase in bound water and sodium within malignant cells. The combination of ultrasound and microwave has provided us a unique opportunity for early-cancer imaging with high resolution and high contrast. We have made significant technical progress in thermoacoustic imaging including imaging configuration, data processing, and reconstruction. We have successfully imaged biological tissue with high resolution and high contrast. We look forward to meeting this grand challenge.

References

1. Y. Xu and L.-H. Wang, "Signal processing in scanning thermoacoustic tomography in biological tissues," Medical Physics 28 (7), 1519–1524 (2001).

2. M. Xu, G. Ku, and L.-H. Wang, "Microwave-induced thermoacoustic tomography using multi-sector scanning," Medical Physics 28 (9), 1958–1963 (2001).

3. D. Feng, Y. Xu, G. Ku, and L.-H. Wang, "Microwave-induced thermoacoustic tomography: reconstruction by synthetic aperture," Medical Physics 28 (12), 2427–2431 (2001).

4. M. Xu, X. Wang, and L.-H. Wang, "High-resolution thermoacoustic tomography of biological tissue," in Biomedical Optoacoustics III, A. A. Oraevsky, ed., Proc. Soc. Photo-Opt. Instrum. Eng. 4618, in press. San Jose, CA, Jan. 20–21, 2002.

Appendices (21 pages)

Appendix 1 (6 pages)

Y. Xu and L.-H. Wang, "Signal processing in scanning thermoacoustic tomography in biological tissues," Medical Physics 28 (7), 1519–1524 (2001).

Appendix 2 (6 pages)

M. Xu, G. Ku, and L.-H. Wang, "Microwave-induced thermoacoustic tomography using multi-sector scanning," Medical Physics 28 (9), 1958–1963 (2001).

Appendix 3 (5 pages)

D. Feng, Y. Xu, G. Ku, and L.-H. Wang, "Microwave-induced thermoacoustic tomography: reconstruction by synthetic aperture," Medical Physics 28 (12), 2427–2431 (2001).

Appendix 4 (4 pages)

M. Xu, X. Wang, and L.-H. Wang, "High-resolution thermoacoustic tomography of biological tissue," in Biomedical Optoacoustics III, A. A. Oraevsky, ed., Proc. Soc. Photo-Opt. Instrum. Eng. 4618, in press. San Jose, CA, Jan. 20–21, 2002.

Signal processing in scanning thermoacoustic tomography in biological tissues

Yuan Xu and Lihong V. Wang[a)]
Optical Imaging Laboratory, Biomedical Engineering Program, Texas A&M University, 3120 TAMU, College Station, Texas 77843-3120

(Received 12 December 2000; accepted for publication 27 March 2001)

Microwave-induced thermoacoustic tomography was explored to image biological tissues. Short microwave pulses irradiated tissues to generate acoustic waves by thermoelastic expansion. The microwave-induced thermoacoustic waves were detected with a focused ultrasonic transducer to obtain two-dimensional tomographic images of biological tissues. The dependence of the axial and the lateral resolutions on the spectra of the signals was studied. A reshaping filter was applied to the temporal piezoelectric signals from the transducer to increase the weight of the high-frequency components, which improved the lateral resolution, and to broaden the spectrum of the signal, which enhanced the axial resolution. A numerical simulation validated our signal-processing approach. © *2001 American Association of Physicists in Medicine.* [DOI: 10.1118/1.1380436]

Key words: microwave, ultrasonics, thermoacoustics, tomography, resolution, filter

I. INTRODUCTION

When electromagnetic radiation is absorbed in biological tissues, the heating and the subsequent expansion will cause emission of acoustic signals, which is called the thermoacoustic effect. In thermoacoustic tomography, the thermoacoustic signals from a tissue sample are collected to map the distribution of the radiative absorption within the sample. The radiative absorption is closely related to the physiological and pathological status of the tissue: for example, cancerous breast tissues are 2–5 times more strongly absorbing to microwaves than surrounding normal breast tissues, which has been attributed to an increase in bound water and sodium within malignant cells.[1–3]

Thermoacoustic tomography combines good imaging resolution with good imaging contrast. Purely microwave imaging has the advantage of good imaging contrast but suffers from poor spatial resolution due to the large wavelength of microwaves.[4–7] On the other hand, purely ultrasonic imaging has good spatial resolution but poor contrast. Thermoacoustic tomography can bridge the gap between them.

There are various types of thermoacoustic tomography, such as photoacoustic tomography and microwave-induced thermoacoustic tomography (MITT). In photoacoustic tomography,[8–11] due to the use of short laser pulses—several nanoseconds in pulse width—and the strong attenuation of the laser light by tissues, the frequency spectrum of the acoustic signal from the buried object of several micrometers in size is estimated to have significant components up to 75 MHz,[9] which makes its axial resolution as good as 10 μm. However, the maximum imaging depth in photoacoustic tomography is limited by the strong attenuation of the laser light and of the high-frequency acoustic waves. On the other hand, MITT can be used to image much deeper tissues due to the relatively low absorption of microwaves. The spectra of the acoustic signals in MITT are usually below 2 MHz, and the axial resolution is greater than 1 mm. Several investigators employed microwave-induced thermoacoustic waves in the 1980s for imaging of biological tissues; these early works, however, did not produce any tomographic or depth-resolved images.[12–14] Recent progress realized tomographic imaging of biological tissues based on microwave-induced thermoacoustic waves.[15–18]

We here present our studies on the signal-processing aspect of scanning MITT. Filtering has been applied to signal processing in photoacoustic tomography[11] and MITT;[15] however, it was used to eliminate the dc (direct current) offset and the effect of the response of the transducer on the piezoelectric signal, respectively. For the first time, we discuss in details how the spectra of signals influence the resolution of thermoacoustic tomography and how the resolution can be improved by signal processing. In our imaging approach, the lateral resolution was achieved by use of a focused ultrasonic transducer, whereas the axial resolution was obtained by measuring the temporal profiles of the acoustic signals. The dominance of the low-frequency (<0.5 MHz) components in the raw temporal signals limited the lateral resolution, and the narrow bandwidth of the signals restricted the axial resolution. Consequently, the image before signal processing had poor lateral resolution and many artifacts. We showed that a "simple" filtering method improved the lateral resolution to some extent but at the expense of the axial resolution. To overcome this problem, we proposed a new reshaping filter. It was applied to the temporal signals from the transducer to increase the weight of the high-frequency components, which improved the lateral resolution, and to broaden the spectrum of the signal, which enhanced the axial resolution. A numerical simulation validated our signal-processing approach.

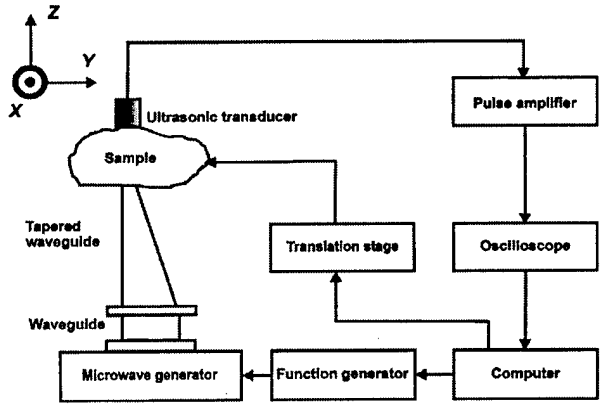

FIG. 1. Experimental setup for scanning MITT.

II. METHODS

A. Experimental setup

The experimental setup for this study is shown in Fig. 1. A Cartesian coordinate system was set up for reference: The x axis pointed outward perpendicularly to the drawing plane, the y axis pointed to the right in the drawing plane, and the z axis pointed upward along the acoustic axis. A 3 GHz microwave generator transmitted microwave pulses. The pulse width was modified from the original manufacturer's setting to 0.5 μs. A function generator was employed to trigger the microwave generator, to control its pulse repetition frequency, and to synchronize the sampling by the oscilloscope. Microwave energy was delivered by a tapered waveguide with a cross section that gradually narrowed from 72 mm $\times$34 mm to 72 mm$\times$5 mm. The object to be imaged was a slab of chicken muscle with a y-z cross section of 14 mm $\times$8 mm, and the slab was plunged into lard contained in a plexiglass tank. The tank was mounted on a two-dimensional (2D) x-y translation stage (MD2, Arrick Robotics), which was driven by two computer-controlled stepper motors. Lard and plexiglass were used for their low absorption to microwaves. Lard also provided good acoustic coupling to an ultrasonic transducer facing the microwave waveguide. The central frequency of the ultrasonic transducer (V314, Panametrics) was 1 MHz, the bandwidth was 0.6 MHz, the diameter of the active element was 1.9 cm, and the focal length was 2.5 cm. The transducer was connected to a low-noise pulse preamplifier. The amplified signal was averaged 100 times, recorded by an oscilloscope (TDS-640A, Tektronix), and then transferred to a personal computer.

In our scanning MITT, the ultrasonic transducer measured the time-of-arrival signals of the thermoacoustic waves. The distances between the thermoacoustic sources and the transducer were calculated by multiplying the time of arrival with the speed of sound in the medium. Therefore, a time-domain signal can be converted into a one-dimensional (1D) image along the acoustic axis (z axis), which is similar to an ultrasonic A-scan image. Scanning the sample along the x or the y axis and combining the multiple 1D images yielded a 2D cross-sectional image of the sample in the x-z or y-z plane, which is analogous to an ultrasonic B-scan image.

B. Signal processing

Two methods of signal processing in the frequency domain based on finite impulse response (FIR) filters were applied to the experimental data. The filtering is implemented by multiplying a properly selected real window function to the spectra of the signals, which introduces no phase distortion. In the first method, all the signals are processed with the same bandpass filter, which has a passband between 0.5 and 1.5 MHz with a transition bandwidth of ~0.5 MHz.

To overcome the difficulties of the first method, we proposed a reshaping method in the frequency domain. This method can make the bandwidth of the processed signal broader to enhance the axial resolution and weigh the high-frequency components more heavily to improve the lateral resolution. The essence of this method is to apply a reshaping filter to each temporal signal. The shape of the reshaping filter for the signal at any y position is chosen to be the inverse of the envelope of the original frequency spectrum, where the envelope of the spectrum is obtained by connecting the major local maxima. Without distorting the positions of the pulses in the temporal signal, this filter can achieve the widest possible bandwidth in the filtered signal and consequently the best axial resolution. Moreover, to filter out the very low-frequency disturbance—which is caused by the preamplifier—and the high-frequency noise beyond the cutoff frequency—where the signal-to-noise ratio is unity, a smoothing filter is applied to the signal. Unlike the reshaping filter, the smoothing filter is the same for the signals from all the scanned positions of the transducer. The final filter is the product of the above two filters in the frequency domain. To increase the contrast, the background value is subtracted from the spectrum before the final filter is applied. Lastly, to improve the lateral resolution, the final filter is scaled by a constant factor such that the spectral amplitudes of all the piezoelectric signals at a selected high frequency remain unchanged after filtering.

III. RESULTS AND DISCUSSION

An image of the chicken muscle is presented in Fig. 2(a). Each vertical line in this 2D image was obtained from a temporal piezoelectric signal of the ultrasonic transducer, and the sample was scanned horizontally along the y axis with a step size of 1 mm to acquire the multiple vertical lines. Figures 2(b) and 2(c) show the temporal wave forms and the corresponding frequency spectra, respectively, for y equal to 20 mm—where the transducer axis crossed the muscle—and equal to 2 mm—where the transducer axis did not cross the muscle. The buried muscle was clearly imaged as shown in Fig. 2(a): The white line at $z=17$ mm corresponds to the upper boundary between the lard and the muscle, and the dark line at $z=25.1$ mm to the lower one. The thickness of the muscle in the image is 8.1 mm and agrees with the actual one. But the lateral resolution is poor: The width of the muscle in the image appears to be 36 mm,

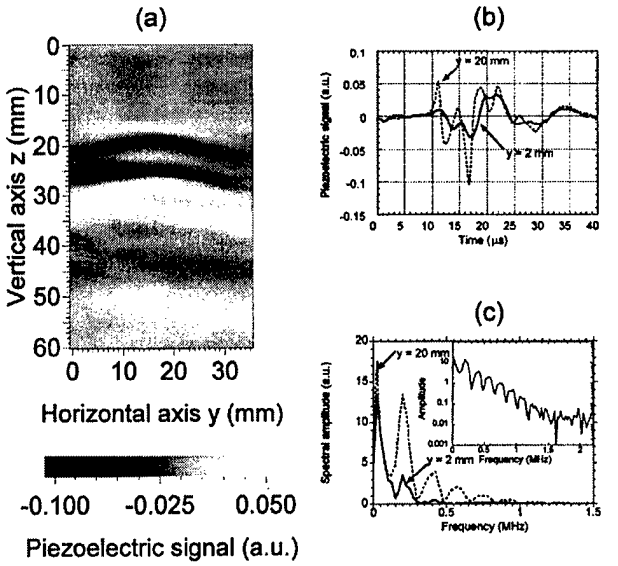

FIG. 2. (a) 2D image of the y-z cross section of the sample obtained by scanning MITT before data processing; (b) temporal microwave-induced thermoacoustic signals at different positions $y=20$ and 2 mm; (c) the main panel shows both of the corresponding spectra on a linear scale, and the inset shows the spectrum for $y=20$ mm on a logarithmic scale.

much greater than the actual 14 mm width. Furthermore, there appear many ghost objects between the two boundaries and below the lower boundary. Because the muscle and the lard are almost uniform, no heterogeneity in the image is expected from other than the boundaries.

To explain these problems, we resort to the relationship between the lateral resolution of the detecting ultrasonic transducer and the frequency spectrum of the received temporal wave form. The lateral resolution of the ultrasonic transducer is determined by its focal diameter, which is given by

$$d_f=\frac{1.02\nu_a l_f}{d_a f_a}, \tag{1}$$

where ν_a is the speed of sound in the medium, l_f is the focal length of the transducer, d_a is the diameter of the active element in the transducer, and f_a is the acoustic frequency.

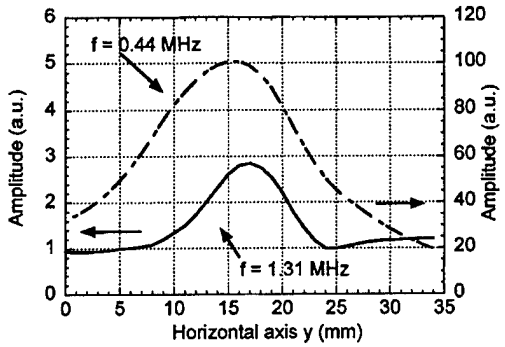

FIG. 3. The distributions of the signal components around $f=1.31$ and 0.44 MHz along the y axis.

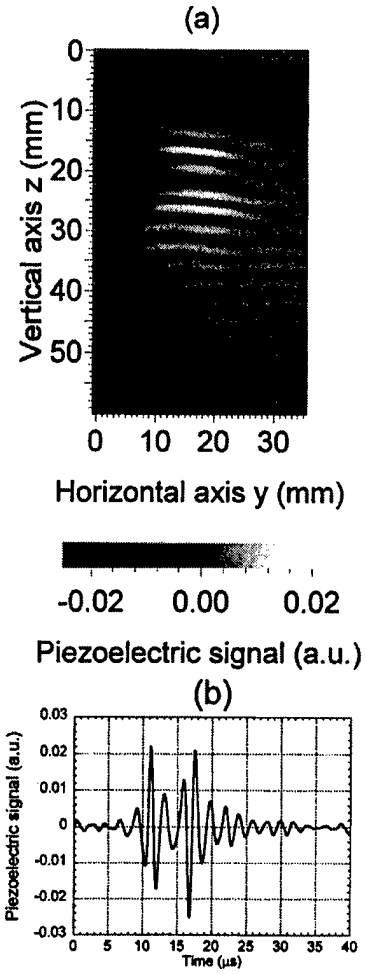

FIG. 4. (a) The 2D image after filtering the temporal signals with a standard bandpass filter; (b) the filtered temporal signal at $y=20$ mm.

Therefore, the lateral resolution is inversely proportional to the frequency of the acoustic signal or the piezoelectric signal. Because the dominant frequency components of the piezo-electrical signals are far below 1 MHz, as shown in Fig. 2(c), the lateral resolution is much worse than the focal diameter of the transducer, 2 mm, at its 1 MHz central frequency.

The dependence of the lateral resolution on the frequency spectra is illustrated more clearly in Fig. 3, which displays the 1D lateral images—along the y axis—corresponding to the 1.31 and 0.44 MHz components of the spectra, respectively. The 1.33 MHz image is sharper than the 0.44 MHz one, and therefore, has superior lateral resolution. Poor resolution that is caused by the dominating low-frequency components is also responsible for the ghost piezoelectric signals at $y=2$ mm, where the transducer axis does not cross the buried muscle and thus the received piezoelectric signals can be only wide-angle low-frequency signals. In comparison, the piezoelectric signal at $y=20$ mm—where the acoustic axis of the transducer crosses the muscle—is primarily from the transducer axis and hence has greater high-frequency

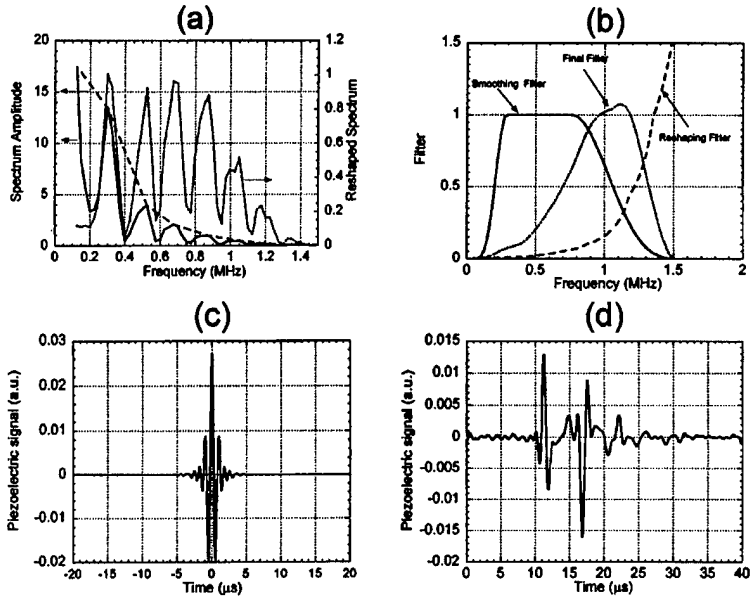

FIG. 5. (a) The envelope (dashed curve) of the spectrum (solid curve) of the temporal signal at $y=20$ mm and the spectrum after the reshaping processing (dotted curve); (b) the reshaping filter—which is the inverse of the envelope, the smoothing filter—which is used to filter the high-frequency noise and the extremely low-frequency signal, and the final filter—which is the product of the reshaping filter and the smoothing filter; (c) the temporal wave form corresponding to the final filter; (d) the temporal wave form corresponding to the spectrum in Fig. 5(a) after the reshaping processing.

components than the piezoelectric signal at $y=2$ mm, as shown in Fig. 2(c).

From the above discussion, it is clear that increasing the high-frequency components of the piezoelectric signals can improve the lateral resolution. The most natural solution is to apply a bandpass filter to cut off the low-frequency components. An example of such processing, in which the filter has a passband between 0.5 and 1.5 MHz with a transition bandwidth of ~0.5 MHz, is shown in Fig. 4(a). The lateral resolution is much improved but still unsatisfactory; however, the axial resolution seems worse, and some artifacts were generated, as shown in Fig. 4(b). The poor axial resolution is due to the decrease of bandwidth in the signal processing. As shown in the inset of Fig. 2(c), the spectral amplitude drops exponentially with the frequency; therefore, the filtered signal has a narrower bandwidth than the original one. A narrower bandwidth in the frequency domain results in a broader signal in the time domain thus poor axial resolution.

To overcome the difficulties of the simply filtering, we applied reshaping filters to the signals. The shape of the reshaping filter [Fig. 5(b)] for the signal at $y=20$ mm is chosen to be the inverse of the envelope of the original frequency spectrum; where the envelope of the spectrum is obtained by connecting the major local maxima, as shown by the dashed curve in Fig. 5(a). Without distorting the positions of the pulses in the temporal signal, this filter can achieve the widest possible bandwidth in the filtered signal and consequently the best axial resolution. Moreover, to filter out the very low-frequency disturbance—which is caused by the preamplifier—and the high-frequency noise beyond the cutoff frequency—where the signal-to-noise ratio is unity, a smoothing filter is applied to the signal. Unlike the reshaping filter, the smoothing filter is the same for the signals from all the scanned positions of the transducer.

The final filter, which is the product of the above two filters in the frequency domain, is shown in Fig. 5(b); the final filter in the time domain is shown in Fig. 5(c). To increase the contrast, the background value—which is determined by the amplitude at both the ends of the solid curve in Fig. 3—is subtracted from the spectrum before applying the final filter. As we wish to obtain a lateral resolution approaching that at 1.31 MHz (Fig. 3), the final filter is scaled by a constant factor such that the spectral amplitude of the final filter at 1.31 MHz is set to unity; consequently, the spectral amplitudes of the piezoelectric signals for all piezoelectric signals remain unchanged at 1.31 MHz. The spectrum and the temporal wave form of the processed signal at $y=20$ mm are displayed in Figs. 5(a) and 5(d). The axial resolution of the processed signal is much better than that of the unprocessed signal [Fig. 2(b)] because the processed spectrum is much broader than the unprocessed one [Fig. 2(c)]. The processed 2D image (Fig. 6) is also clearer than the original image. The ghost objects in the original images were removed, and the two boundaries became quite distinct from the background. The muscle along the y axis in the image is about 15 mm, which agrees well with the 14 mm actual size.

A numerical simulation was implemented to test our reshaping method. A simulated temporal waveform [Fig. 7(a)] includes three pulses at $t=20$, 21, and 30 μs. The 20 and 30 μs pulses are determined by

$$s(t)=\exp\left(-\frac{(t-t_0)^2}{w^2}\right), \tag{2}$$

and the 21 μs pulse is determined by

$$s(t)=1\Big/\left(1+\frac{(t-t_0)^2}{w^2}\right), \tag{3}$$

where w is the pulse width and is set to 0.8 μs. The corresponding spectrum is shown in Fig. 7(b), which resembles the spectrum of the signal at $y=20$ mm in our image. Be-

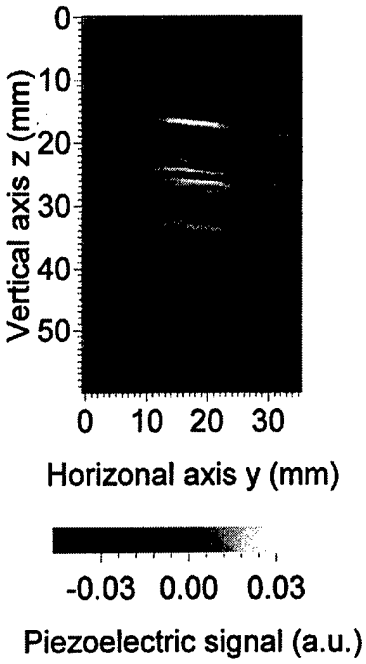

FIG. 6. The 2D image after applying the final filter to the temporal piezoelectric signals.

cause the 20 and 21 μs pulses are too close to each other, they merge into one pulse in the original constructed signal. In the signal processed by our method [Fig. 7(c)], the two pulses are separated distinctively, and all the pulses become sharper. The positioning errors of the restored peaks are within 10% of the pulse width. However, the signal-to-noise ratio (SNR) in Fig. 7(c) is lower than that in Fig. 7(a) as a result of the increased weighting of the noisy high-frequency components in the reshaping process. Nevertheless, the degradation of SNR in the processed signals has little influence on the image, as shown in Fig. 6. In contrast, the simple filtering did not produce as a good outcome [Fig. 7(d)].

Our reshaping method is especially efficient for signals that consist of multiple pulses of similar shapes, which is quite common in ultrasonic detection. Assuming a temporal signal comprises two identical pulses—for illustration purposes—at different times, its spectral amplitude can be written as

$$A(f)=s(f)|1+\exp(i2\pi f\Delta t)|=s(f)p(f), \tag{4}$$

where f is the frequency, $s(f)$ is the spectral amplitude of a single pulse, and Δt is the time interval between the two pulses. Because the oscillatory $p(f)$ has a flat envelope, the envelope of $A(f)$ approximately equals that of $s(f)$, which determines the shape of a single pulse. On the other hand, the features and the phase of the spectrum contain the positioning information of the pulses, which is the most important information in imaging. In our reshaping method, the signal is multiplied by the reciprocal of its own spectral envelope, resulting in a flat envelope in the processed spectrum; consequently, the pulses are narrowed in the time domain. As the reshaping filter is smooth, it does not alter the features and the phase of the spectrum; accordingly, the positions of the pulses in the time domain remain unchanged.

In general, applying the reshaping filter will sharpen the boundaries of signals, which can be illustrated with an ideal slab. The thermoacoustic wave from a slab irradiated by a sufficiently short microwave pulse can be represented by a square wave. It can be shown that filtering the square wave with the reshaping filter is equivalent to taking the first derivative of the wave in the time domain, which yields the two boundaries of the slab. The spectral amplitude of the square wave with a duration a is $|\sin(\pi af)/(\pi f)|$; thus its envelope is $1/(\pi f)$, and the reshaping filter is πf. Applying the reshaping filter to the square wave in the frequency domain is

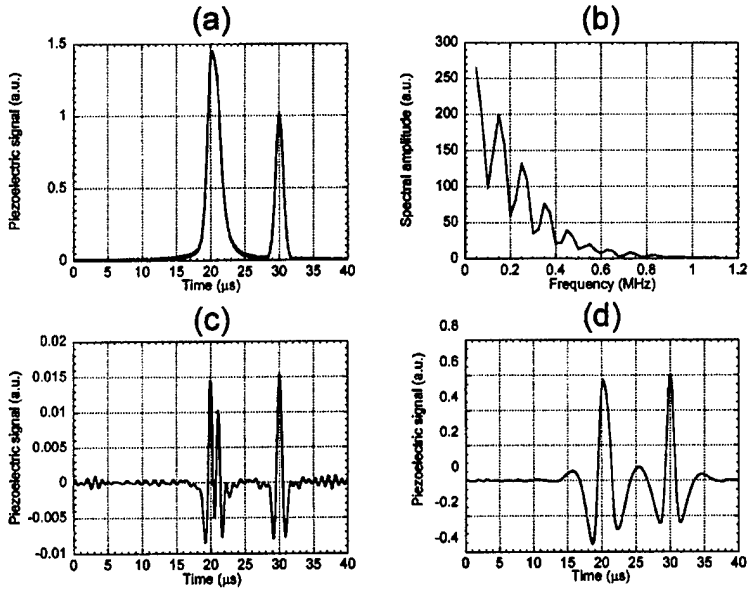

FIG. 7. (a) The simulated piezoelectric signal; (b) the corresponding spectrum; (c) the piezoelectric signal after reshaping the spectrum; (d) the piezoelectric signal after applying the smoothing filter as shown in Fig. 5(b).

equivalent, within a constant factor, to differentiating the signal in the time domain, which yields a positive delta function at the front boundary of the square wave and a negative one at the rear boundary.

Our study pointed out some potential approaches that can be used to improve the imaging resolution in our experiments. One approach is to improve the SNR of the signal so that the cutoff frequency is extended. Because only the spectral region with an SNR greater than unity provides useful information for our reshaping method, an increased cutoff frequency can broaden the usable spectrum and accordingly improve both the lateral and the axial resolutions. However, this advantage can only be realized when the spectrum is reshaped because the unprocessed high-frequency spectral amplitude is so small compared with the low-frequency one that it contributes little to improving the lateral and the axial resolutions, as shown in Fig. 2(c); after the reshaping, the weight of the high-frequency portion is increased greatly, resulting in an improved resolution. Another potential approach to improving the resolution is to shift the acoustic spectrum to a higher frequency by modulating the microwave source.

IV. CONCLUSIONS

Our studies showed that scanning MITT is a promising imaging tool for biological tissues. The boundaries of different tissue constituents can be imaged clearly and accurately with the assistance of image processing. By reshaping the spectra of the piezoelectric signals, the weight of the high-frequency components is increased greatly, resulting in much improved axial and lateral resolutions, both of which were 1 mm in our current experimental setup. The numerical simulation also verified our signal-processing method. Our spectral-reshaping method can also be applied to other ultrasonic signals comprising several pulses of similar shapes.

ACKNOWLEDGMENTS

We thank G. Ku for experimental assistance. This project was sponsored in part by the U.S. Army Medical Research and Materiel Command Grant No. DAMD17-00-1-0455, the National Institutes of Health Grants No. R01 CA71980 and No. R21 CA83760, the National Science Foundation Grant No. BES-9734491, and Texas Higher Education Coordinating Board Grant No. ARP 000512-0123-1999.

[a]Author to whom all correspondence should be addressed. Telephone: 979-847-9040; Fax: 979-845-4450; Electronic mail: LWang@tamu.edu; URL:http://oilab.tamu.edu

[1] W. Joines, R. Jirtle, M. Rafal, and D. Schaeffer, "Microwave power absorption differences between normal and malignant tissue," Int. J. Radiat. Oncol., Biol., Phys. **6**, 681–687 (1980).

[2] S. Chaudhary, R. Mishra, A. Swarup, and J. Thomas, "Dielectric properties of normal human breast tissues at radiowave and microwave frequencies," Indian J. Biochem. Biophys. **21**, 76–79 (1984).

[3] W. Joines, Y. Zhang, C. Li, and R. Jirtle, "The measured electrical properties of normal and malignant human tissues from 50–900 MHz," Med. Phys. **21**, 547–550 (1994).

[4] *Medical Applications of Microwave Imaging*, edited by L. E. Larsen and J. H. Jacobi (IEEE, Piscataway, NJ, 1986).

[5] S. Caorsi, A. Frattoni, G. L. Gragnani, E. Nortino, and M. Pastorino, "Numerical algorithm for dielectric-permittivity microwave imaging of inhomogeneous biological bodies," Med. Biol. Eng. Comput. **29**, NS37–NS44 (1991).

[6] M. S. Hawley, A. Broquetas, L. Jofre, J. C. Bolomey, and G. Gaboriaud, "Microwave imaging of tissue blood content changes," J. Biomed. Eng. **13**, 197–202 (1991).

[7] P. M. Meaney, K. D. Paulsen, and J. T. Chang, "Near-field microwave imaging of biologically-based materials using a monopole transceiver system," IEEE Trans. Microwave Theory Tech. **46**, 31–45 (1998).

[8] R. A. Kruger, P. Liu, Y. R. Fang, and C. R. Appledorn, "Photoacoustic ultrasound (PAUS)—reconstruction tomography," Med. Phys. **22**, 1605–1609 (1995).

[9] C. G. A. Hoelen, F. F. M. Demul, R. Pongers, and A. Dekker, "Three-dimensional photoacoustic imaging of blood vessels in tissue," Opt. Lett. **23**, 648–650 (1998).

[10] A. A. Karabutov, E. V. Savateeva, N. B. Podymova, and A. A. Oraevsky, "Backward mode detection of laser-induced wide-band ultrasonic transients with optoacoustic transducer," J. Appl. Phys. **87**, 2003–2014 (2000).

[11] C. G. A. Hoelen, R. Pongers, G. Hamhuis, F. F. M. Demul, and J. Greve, "Photoacoustic blood cell detection and imaging of blood vessels in phantom tissue," Proc. SPIE **3196**, 142–153 (1998).

[12] T. Bowen, L. Nasoni, A. E. Pifer, and G. H. Sembrosk, "Some experimental results on the thermoacoustic imaging of soft tissue-equivalent phantoms," Proc.-IEEE Ultrason. Symp. **2**, 823–827 (1981).

[13] R. G. Olsen and J. C. Lin, "Acoustic imaging of a model of a human hand using pulsed microwave irradiation," Bioelectromagnetics (N.Y.) **4**, 397–400 (1983).

[14] J. C. Lin and K. H. Chan, "Microwave thermoelastic tissue imaging—system design," IEEE Trans. Microwave Theory Tech. **32**, 854–860 (1984).

[15] R. A. Kruger, D. R. Reinecke, and G. A. Kruger, "Thermoacoustic computed tomography—technical considerations," Med. Phys. **26**, 1832–1837 (1999).

[16] L.-H. V. Wang, X. Zhao, H. Sun, and G. Ku, "Microwave-induced acoustic imaging of biological tissues," Rev. Sci. Instrum. **70**, 3744–3748 (1999).

[17] G. Ku and L.-H. V. Wang, "Scanning thermoacoustic tomography in biological tissue," Med. Phys. **27**, 1195–1202 (2000).

[18] G. Ku and L.-H. V. Wang, "Scanning microwave-induced thermoacoustic tomography: signal, resolution, and contrast," Med. Phys. **28**, 4–10 (2001).

Microwave-induced thermoacoustic tomography using multi-sector scanning

Minghua Xu, Geng Ku, and Lihong V. Wang[a)]
Optical Imaging Laboratory, Biomedical Engineering Program, Texas A&M University, 3120 TAMU, College Station, Texas 77843-3120

(Received 26 March 2001; accepted for publication 18 June 2001)

A study of microwave-induced thermoacoustic tomography of inhomogeneous tissues using multi-sector scanning is presented. A short-pulsed microwave beam is used to irradiate the tissue samples. The microwave absorption excites time-resolved acoustic waves by thermoelastic expansion. The amplitudes of the acoustic waves are strongly related to locally absorbed microwave-energy density. The acoustic waves may propagate in all spatial directions. A focused ultrasonic transducer is employed to acquire temporal acoustic signals from multiple directions. Each detected signal is converted into a one-dimensional (1D) image along the acoustic axis of the transducer. The cross-sectional images of the tissue samples are calculated by combining all of the 1D images acquired in the same planes. © *2001 American Association of Physicists in Medicine.*
[DOI: 10.1118/1.1395037]

Key words: microwave, thermoacoustics, tomography, imaging, sector, scan

I. INTRODUCTION

Microwave-induced thermoacoustic tomography of biological tissues has recently attracted considerable interest.[1–3] With this technique, a short-pulsed microwave beam is used to irradiate tissue samples. The tissue absorbs the microwave energy and excites thermoacoustic waves by thermoelastic expansion. The generated acoustic waves carry information about the microwave absorption properties of the sample. The different absorption properties among different types of tissue permit the construction of a distribution of microwave absorption in a homogeneous acoustic medium.

The microwave penetration depth in most soft tissues lies somewhere between that of the fat tissue, which lacks water and salt, and muscle tissue, which is abundant in water and salt.[2] Specifically, the penetration depths for fat and muscle tissue at 3-GHz microwave are 9 cm and 1.2 cm, respectively. The wide range of microwave absorption coefficients among various other tissues can lead to a high imaging contrast for biological tissues. However, it is difficult to achieve good spatial resolution using pure microwave imaging of biological tissues because of the long wavelength of microwaves, e.g., 3 cm at 3 GHz.[4,5] This problem can be overcome by the use of microwave-induced thermoacoustic waves. Because the velocity of acoustic waves in soft tissue is nearly 1.5 mm/μs, thermoacoustic signals at mega Hz can provide millimeter spatial resolution.

The intensities of the microwave-induced thermoacoustic signals are far lower than the ultrasonic pulses used in purely ultrasound imaging (ultrasonography). However, a unique advantage of thermoacoustic tomography is the detection of the inhomogeneous microwave absorption property of tissues when the acoustic property is homogeneous. Such a capability may lead to early detection of cancer.

Key problems in microwave-induced thermoacoustic tomography are the measurement of acoustic signals excited by microwave pulses and the construction of images from the acquired data. One approach is to use focused ultrasonic transducers to localize the thermoacoustic sources. The mature scanning techniques (linear and sector scans) in ultrasonography can be used to detect the thermoacoustic signals.[6] Each scan line may reflect the profile of the medium along the acoustic axis of the focused transducer. However, an acoustic source has a strong direction of radiation, especially if the surface is relatively smooth, from which the acoustic energy is mainly transmitted out in one direction. The higher the frequency of the acoustic wave is, the stronger the radiation direction is. The thermoacoustic signals caused by microwave pulses are composed of high-frequency components as well as low-frequency components, and the intensities of the high-frequency components are far less than the ultrasonic pulses used in ultrasonography. Only if its acoustic axis is nearly perpendicular to the surface of the acoustic source, can the focused transducer acquire enough high-frequency components for accurate spatial localizations of the thermoacoustic sources. Therefore, it is necessary, with this method, to scan the sample from all possible directions by a focused transducer. Since the thermoacoustic wave is weak, in order to get a good signal-and-noise ratio (SNR), we use a focused transducer with a big aperture area in our initial study, because the SNR is proportional to the square root of the aperture area.

Here we present our study on microwave-induced thermoacoustic tomography of inhomogeneous tissues by a two-dimensional (2D) full-directional scan—the combination of multiple-sector scans at various positions on a circle around the sample. Each detected time-resolved signal is converted into a one-dimensional image along the acoustic axis. The axial resolution is obtained by measuring the temporal profiles of the acoustic signals, and the lateral resolution is mainly determined by the focal diameter of the transducer.

The two-dimensional (2D) cross-sectional images are calculated from the data acquired in the same planes. Some images of biological-tissue samples are achieved experimentally. These images clearly reveal the boundaries of different tissues as well as their locations, which are in good agreement with the actual samples.

II. THEORY

A. Thermoacoustic wave

When the microwave pulse duration is very short, the thermal conduction time is far greater than the thermoacoustic transit time. In practice, the duration of the microwave pulse is less than 1 μs, which meets this criterion.[1] In this case, the heat diffusion's effect to the thermoacoustic wave in the tissue can be neglected. Consequently, the generation of thermoacoustic wave by deposition of microwave energy can be described by the following equation:[7]

$$\left(\nabla^2-\frac{1}{c^2}\frac{\partial^2}{\partial t^2}\right)p(\mathbf{r},t)=-\frac{\beta}{C_p}\frac{\partial I(t)}{\partial t}A(\mathbf{r}), \tag{1}$$

where $p(\mathbf{r},t)$ is the thermoacoustic pressure at position $\mathbf{r}$ and time t, c is the speed of sound, β is the isobaric volume expansion coefficient, C_p is the heat capacity, $I(t)$ is the temporal profile of the microwave pulse, and $A(\mathbf{r})$ is the fractional energy-absorption per unit volume of soft tissue at position $\mathbf{r}$, which is proportional to the microwave absorption coefficient of the tissue at position $\mathbf{r}$.

Equation (1) shows that the amplitudes of the thermoacoustic waves are strongly related to locally absorbed microwave-energy density, i.e., the local microwave absorption coefficient or penetration depth. Considering a spherically symmetric deposition of microwave energy with radius R,

$$A(r)=A_0U(-r+R), \tag{2}$$

where the step function

$$U(\xi)=\begin{cases}1, & \xi\geqslant 0,\\ 0, & \xi<0.\end{cases}$$

Assuming a delta pulse of the form $I(t)=I_0\delta(t)$, the thermoacoustic pressure at detection position r for $t>0$ is found from Eq. (1) to be[7]

$$p(r,t)=\frac{\beta I_0c^2}{C_p}\frac{A_0}{2r}(r-ct)[U(-r+R+ct)+U(r+R-ct)]. \tag{3}$$

Moreover, the first derivative of the thermoacoustic pressure is written as

$$\frac{\partial p(r,t)}{\partial t}=-\frac{\beta I_0c^3}{2rC_p}A_0U(-|ct-r|+R). \tag{4}$$

Equation (4) indicates that the first derivative of the thermoacoustic pressure is a mapping of the spherically spatial energy deposition of Eq. (2). Therefore, we can use either the detected thermoacoustic pressure or its first derivative to construct the microwave absorption distribution and the latter is found to be better. In general, a large medium can be regarded as a set of small media or thermoacoustic sources, which have different microwave absorption coefficients. Through the following multi-sector scan method, each small thermoacoustic source can be localized.

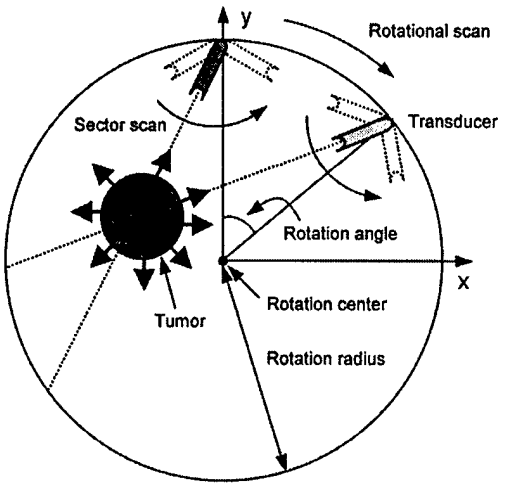

FIG. 1. A diagram of the multi-sector scan scheme.

B. Multi-sector scan

A diagram of the 2D multi-sector scanning scheme is shown in Fig. 1. A rectangular coordinate system (x,y) is set up for reference. Each sector-scan frame has a set of scan lines, which originate from the same location and radiate out in different directions as in ultrasonography. The origins of different frames are set on a circle around the sample so that the focused transducer may detect the signals from all directions in the same plane. For convenience, the center and radius of the circle are referred to as the rotation center and the rotation radius, respectively.

The microwave absorption and sample heating occur in a very short time, and the propagation velocity of the electromagnetic wave is far greater than that of an ultrasonic one. Therefore, it is reasonable to assume that the sample expansion resulting from the microwave pulses causes acoustic waves instantaneously. The distance between the thermoacoustic source and the transducer is simply calculated by multiplying the time of arrival by the velocity of the acoustic wave. Therefore, at each scan line, the thermoacoustic pressure along the acoustic axis induced by the microwave pulses can be obtained directly from the detected temporal signals.

All scan lines are used to construct a cross-sectional image by the method of linear interpolation. A sector frame can only detect part of the sound source. Figure 2(a) shows the same $x-y$ plane as in Fig. 1. The transducer is now set at the position of point O_1. A local polar coordinate system (d,α) is set up for the sector frame with the origin O_1, and its polar axis is through the rotation center point O. The angle θ between the polar axis and y axis is called the rotation angle.

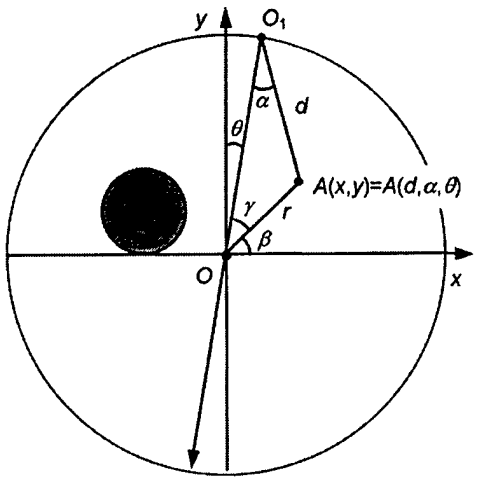

(a)

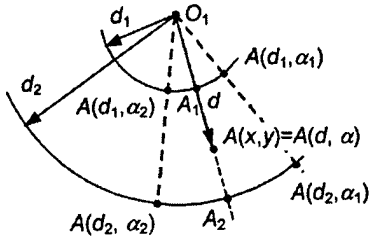

(b)

FIG. 2. (a) The rectangular coordinate system (x,y) and the local polar coordinate system (d,α,θ); (b) the diagram of the linear interpolation.

The rotation radius between point O and O_1 is R. The distance between the thermoacoustic source and the transducer is d. Therefore, at each scan line, the point $A(x,y)$ in the rectangular coordinate system can be denoted as $A(d,\alpha,\theta)$ in the local polar coordinate system with rotation angle θ. The relationship between (x,y) and (d,α,θ) is determined by the following equations:

$$
\begin{aligned}
&d=\sqrt{r^2+R^2-2rR\cos\gamma},\\
&\theta=\arcsin(r\sin\gamma/d),\\
&\beta=\arctan(y/x),\\
&\gamma=\pi/2-\alpha-\beta,\\
&r=\sqrt{x^2+y^2}.
\end{aligned}
\tag{5}
$$

In experiments, a series of discrete data are acquired in each local polar coordinate system. We use linear interpolations to project the data from each local polar coordinate system to the rectangular coordinate system. For simplicity, we neglect the symbol θ in the following description. As shown in Fig. 2(b), suppose that point (d,α) is among the measured data $A(d_1,\alpha_1)$, $A(d_2,\alpha_1)$, $A(d_1,\alpha_2)$, and $A(d_2,\alpha_2)$, i.e., $\alpha_1 \leqslant \alpha \leqslant \alpha_2$, $d_1 \leqslant d \leqslant d_2$, where $d_i\,(i=1,2)$ is the distance between the thermoacoustic source and the transducer and is calculated by multiplying the time of arrival $t_i\,(i=1,2)$ by the velocity of the acoustic wave c in the medium, i.e., $d_i = ct_i\,(i=1,2)$. Then $A(d,\alpha)$ can be calculated by

$$
\begin{aligned}
A(d,\alpha)&=\frac{d-d_1}{d_2-d_1}(A_2-A_1)+A_1,\\
A_1&=A(d_1,\alpha_1)+\frac{A(d_1,\alpha_2)-A(d_1,\alpha_1)}{\alpha_2-\alpha_1}\times(\alpha-\alpha_1),\\
A_2&=A(d_2,\alpha_1)+\frac{A(d_2,\alpha_2)-A(d_2,\alpha_1)}{\alpha_2-\alpha_1}(\alpha-\alpha_1).
\end{aligned}
\tag{6}
$$

Function A could be the thermoacoustic pressure $p(t)$ or the derivative $dp(t)/dt$. The derivative is helpful for improving the sharpness of the boundaries between different tissues, which can be calculated through an inverse fast Fourier transformation (FFT) as

$$
\frac{dp(t)}{dt}=\mathrm{FFT}^{-1}\{i\omega p(\omega)\},
\tag{7}
$$

where $p(\omega)$ is the Fourier transformation of $p(t)$.

In this way, we can compute each image $A_\theta(x,y)$ from each sector frame $A(d,\alpha)$ at rotation angle θ. A full 2D cross-sectional image is obtained with the following summation:

$$
A(x,y)=\sum_{\theta} A_\theta(x,y).
\tag{8}
$$

III. EXPERIMENTAL METHOD

We use a focused transducer to implement a multi-sector scan. Figure 3 shows the experimental setup. A plexiglass container is filled with mineral oil. A rotation stage and a focused transducer are immersed inside it in the same $x-y$ plane. The sample can be set in the rotation stage. The transducer is used to detect the thermoacoustic signal from the sample. The angle panel indicates the angle between the acoustic axis of the transducer and the rotation radius. We manually turn the transducer to point to one direction. A step motor directly drives the rotation stage while the transducer is fixed. Obviously, this is equivalent to a transducer that rotationally scans around the sample with a manual sector scan. The transducer (V314, Panametrics) has a central frequency of 1 MHz, a bandwidth of 0.6 MHz, a diameter of 1.9 cm, a focal length of 2.5 cm at 1 MHz, a 3-dB focal diameter of 2.1 mm, and a focal zone of 1.76 cm along the acoustic axis.

The microwave pulses transmitted from a 3-GHz microwave generator have a pulse energy of 10 mJ and a pulse width of 0.5 μs. A function generator (Protek, B-180) is used to trigger the microwave generator, control its pulse repetition frequency, and synchronize the oscilloscope sampling. Microwave energy is delivered to the sample by a rectangular wave guide with a cross section of 72 mm×34 mm.

A personal computer is used to control the step motor in rotating the sample. The signal from the transducer is first amplified through a pulse amplifier, then recorded and aver-

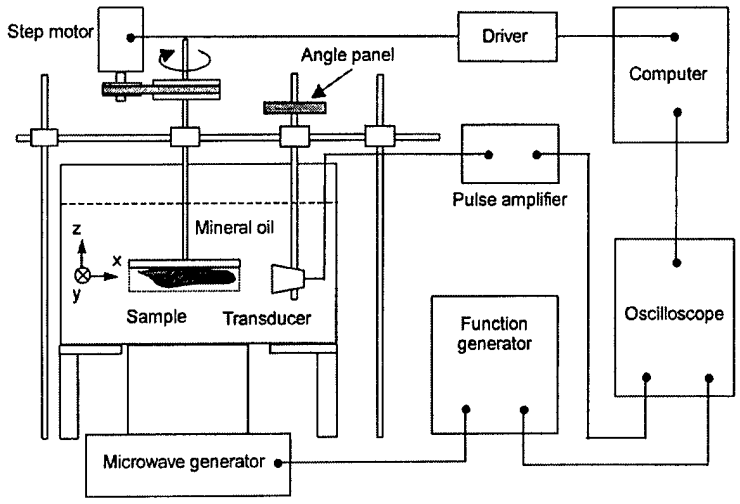

FIG. 3. Experimental setup.

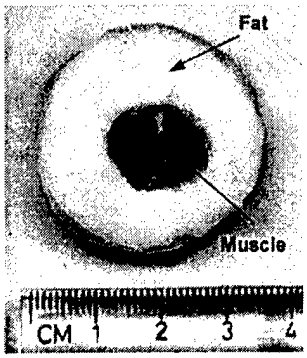

(a)

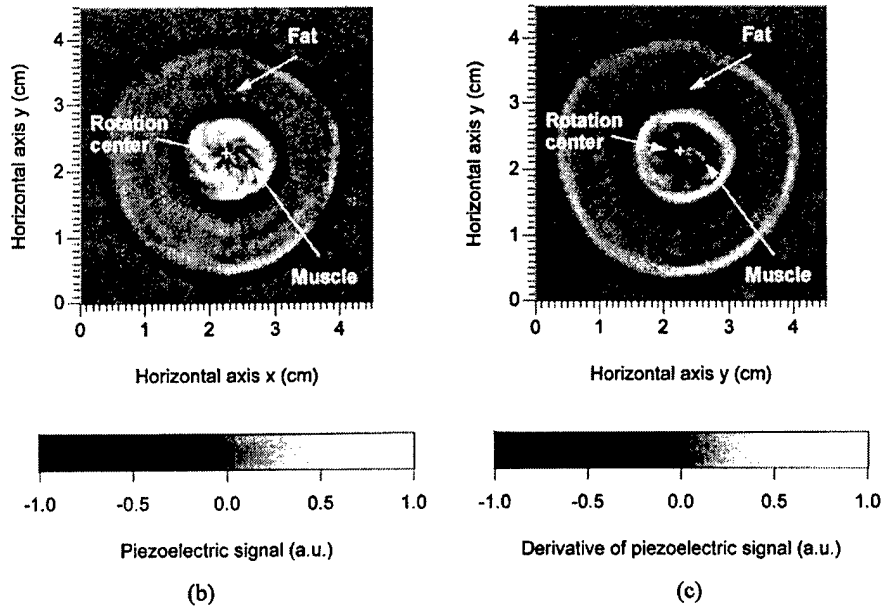

FIG. 4. (a) Cross section of a sample on the $x-y$ plane; 2D constructed images of the $x-y$ cross section of the sample (b) from the piezoelectric signals and (c) from the first derivative of the piezoelectric signals.

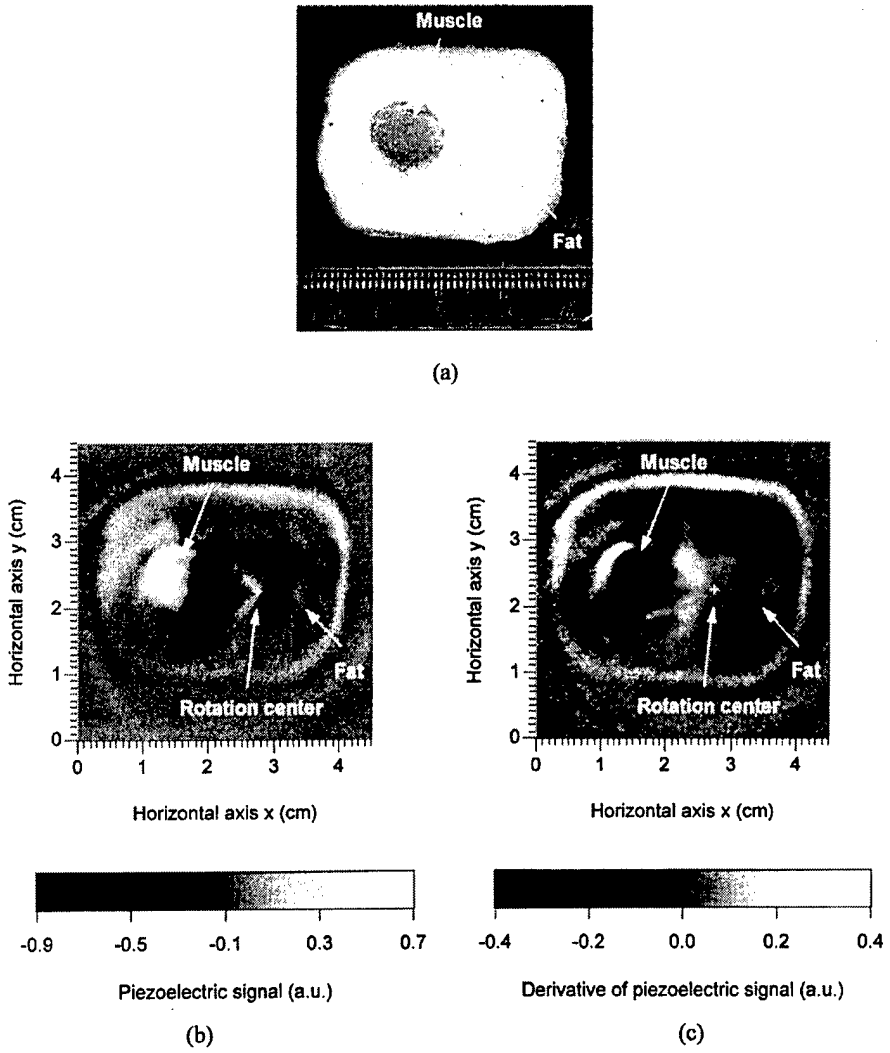

FIG. 5. (a) Cross section of a sample on the $x-y$ plane; 2D constructed images of the $x-y$ cross section of the sample (b) from the piezoelectric signals and (c) from the first derivative of the piezoelectric signals.

aged 100 times by an oscilloscope (TDS640A, Tektronix), and finally transferred to a personal computer for imaging.

IV. RESULTS AND DISCUSSION

The first sample we tested was a piece of muscle tissue—centered in a fat disc as shown in Fig. 4(a)—which was cut across and photographed after the experiment. Both the muscle and fat were cut from pork. The maximum diameter of the sample was 38 mm, and the thickness was 5 mm. The rotation center was set inside the muscle. The transducer rotationally scanned the sample (only in the rotation-radius directions) from 0 to 360 degrees with a step size of 2.25 degrees. We then used these 160 scan lines to calculate a 2D cross-sectional image with linear interpolations. Good agreement between the original profile in Fig. 4(a) and the constructed images in Figs. 4(b) and 4(c) was obtained, where Figs. 4(b) and 4(c) were computed from the measured piezoelectric signals and the first derivative of those, respectively. The boundaries between the fat and muscle or oil are clearly imaged. This is because when the rotation center is in the center of the sample, each scan line is nearly perpendicular to the boundaries of the muscle or fat, and the transducer can receive sufficient thermoacoustic signals from the radius directions alone for imaging.

The second sample had a structure as shown in Fig. 5(a), which was also cut across and photographed after the experiment. The fat was first cut from pork: the maximum diameter of the sample was 39 mm; and the thickness was 5 mm. Then we cut away a hole far away from its center and filled in a small piece of muscle, which was also cut from pork. The muscle size was about 10 mm in diameter and 5 mm in thickness. The rotation center was set outside the muscle. The rotation radius was 12.5 cm, which included the length of the transducer. The transducer rotationally scanned the sample from 0 to 360 degrees with a step size of 2.25 degrees, and at each stop a set of sector directions from -12 to 12 degrees with a step size of 2 degrees was scanned. Totally, 2080 scan lines were acquired to construct 2D cross-section images. Figure 5(b) was constructed directly from the piezoelectric signals, which was in good agreement with the origi-

nal profile in Fig. 5(a). The boundaries between the fat and muscle or oil are clearly visible, except the rear boundary of the muscle. Figure 5(c) was constructed from the first derivatives of the piezoelectric signals, which agreed with the original profile of Fig. 5(a) very well. The boundary of the muscle was clearer than that in Fig. 5(b). In particular, the sizes and locations of the muscle and fat zones agreed with the original shapes. It indicates that the first derivative produces a better mapping of the microwave absorption distribution than the piezoelectric signal, i.e., the thermoacoustic pressure. Due to the high microwave absorption in muscle and the low absorption in fat, the muscle and fat can be differentiated by their "brightness" in the images.

In the above examples, the size deviations between the original objects and their constructed images are about 2 mm, which agree with the theoretical spatial resolution approximations as follows. The axial resolution along the acoustic axis is dependent on the width of the microwave pulse (0.5 μs) plus the width of the impulse response of the transducer (1.5 μs); therefore, it should be approximately 3 mm, because the velocity of the acoustic waves in the tissue is about 1.5 mm/μs. The lateral resolution is determined by the focal diameter of the focused transducer, ~2 mm for the 1 MHz transducer used in the above experiments. The use of shorter microwave pulses and narrower focal diameter ultrasonic transducers can improve the spatial resolution.[3]

V. CONCLUSION

Microwave-induced thermoacoustic tomography of inhomogeneous tissues by using multiple sector scans was studied. Cross-sectional images can be obtained by a few straightforward calculations from the temporal data acquired by a focused transducer rotationally sector scanning the samples. The experiments show that the constructed images are in good agreement with the original cross-section profiles of the samples, and the boundaries between different tissues are clearly imaged. Results indicate that this technique is a powerful imaging method with good spatial resolution that can be used for the investigation of inhomogeneous tissues. In the future, a circular array could be used to replace the single transducer, and some numerical compensation methods could be introduced to improve the spatial resolution further.

ACKNOWLEDGMENTS

This project was sponsored in part by the U.S. Army Medical Research and Materiel Command Grant No. DAMD17-00-1-0455, the National Institutes of Health Grant No. R01 CA71980, the National Science Foundation Grant No. BES-9734491, and Texas Higher Education Coordinating Board Grant No. ARP 000512-0123-1999.

[a]Author to whom all correspondence should be addressed. Electronic mail: lwang@tamu.edu; URL:http://oilab.tamu.edu

[1] R. A. Kruger, K. K. Kopecky, A. M. Aisen, D. R. Reinecke, G. A. Kruger, and W. L. Kiser, "Thermoacoustic CT with radio waves: A medical imaging paradigm," Radiology **211**, 275–278 (1999).

[2] G. Ku and L. V. Wang, "Scanning thermoacoustic tomography in biological tissues," Med. Phys. **27**, 1195–1202 (2000).

[3] G. Ku and L. V. Wang, "Scanning microwave-induced thermoacoustic tomography: Signal, resolution, and contrast," Med. Phys. **28**, 4–10 (2001).

[4] *Medical Applications of Microwave Imaging*, edited by L. E. Larsen and J. H. Jacobi (IEEE, Piscataway, NJ, 1986).

[5] P. M. Meaney, K. D. Paulsen, and J. T. Chang, "Near-field microwave imaging of biologically-based materials using a monopole transceiver system," IEEE Trans. Microwave Theory Tech. **46**, 31–45 (1998).

[6] P. N. T. Wells, "Ultrasonic imagining of the human body," Rep. Prog. Phys. **62**, 671–722 (1999).

[7] G. J. Diebold, T. Sun, and M. I. Khan, Photoacoustic waveforms generated by fluid bodies, in *Photoacoustic and Photothermal Phenomena III*, edited by D. Bicanic (Springer-Verlag, Berlin, Heidelberg, 1992), pp. 263–269.

Microwave-induced thermoacoustic tomography: Reconstruction by synthetic aperture

Dazi Feng, Yuan Xu, Geng Ku, and Lihong V. Wang[a)]
Optical Imaging Laboratory, Biomedical Engineering Program, Texas A&M University, 3120 TAMU, College Station, Texas 77843-3120

(Received 14 May 2001; accepted for publication 20 September 2001)

We have applied the synthetic-aperture method to linear-scanning microwave-induced thermoacoustic tomography in biological tissues. A nonfocused ultrasonic transducer was used to receive thermoacoustic signals, to which the delay-and-sum algorithm was applied for image reconstruction. We greatly improved the lateral resolution of images and acquired a clear view of the circular boundaries of buried cylindrical objects, which could not be obtained in conventional linear-scanning microwave-induced thermoacoustic tomography based on focused transducers. Two microwave sources, which had frequencies of 9 and 3 GHz, respectively, were used in the experiments for comparison. The 3 GHz system had a much larger imaging depth but a lower signal–noise ratio than the 9 GHz system in near-surface imaging. © *2001 American Association of Physicists in Medicine.* [DOI: 10.1118/1.1418015]

Key words: thermoacoustics, tomography, synthetic aperture, microwave

I. INTRODUCTION

Microwave-induced thermoacoustic tomography is emerging as a nonionizing imaging modality. When electromagnetic radiation is irradiated upon biological tissues, the resulting heat-related expansion of the tissues produces acoustic waves. From the acoustic signals, we can reconstruct the distribution of electromagnetic absorption in soft tissues. The large differences in electromagnetic absorption in various tissues, which are associated with their physiological and pathological status, provide significant contrasts in imaging. For example, the absorption coefficient in cancerous breast tissue is two to five times greater than that in normal breast tissue, due to the increment of water and sodium bounded within malignant cells.[1–3] This large difference makes it promising to use microwave-induced thermoacoustic tomography to detect breast cancers.

Microwave-induced thermoacoustic tomography combines the advantages of both pure ultrasound and pure microwave imaging. Traditional imaging technology with pure ultrasound (ultrasonography) offers satisfactory spatial resolution but poor soft-tissue contrast, while pure microwave imaging provides good imaging contrast but barren spatial resolution.[4–7] Microwave-induced thermoacoustic tomography bridges the gap between them. By integrating ultrasound and microwave technology, microwave-induced thermoacoustic tomography has both satisfactory spatial resolution and good soft-tissue contrast.

In conventional linear-scanning microwave-induced thermoacoustic tomography (LMTT), a focused ultrasonic transducer is used to detect time-resolved acoustic signals. Since the focused transducer has a good response only along the transducer axis, each acoustic signal can be converted into a one-dimensional image. Linear scanning of the ultrasonic transducer yields multiple one-dimensional images, which can be combined to form a two-dimensional image of the sample.[8–10] In the two-dimensional images obtained with conventional LMTT, only boundaries that are nearly perpendicular to the axis of the ultrasonic transducer can be detected because most of the thermoacoustic waves travel in a small solid angle around the normals of boundaries; spherical or oblique boundaries of buried objects whose thermoacoustic waves have a large angle with the axis of the ultrasonic transducer cannot be imaged because the ultrasonic transducer receives little signal from these boundaries.

To overcome this deficiency of traditional LMTT, we have applied the synthetic-aperture method to LMTT. In this method, thermoacoustic signals were detected from multiple locations and the synthetic delay-and-sum algorithm was then used for the reconstruction of the images. The synthetic-aperture method has been applied in PAT previously;[11–14] and weights were assigned to the signals according to the sensor's directivity to improve the SNR at the expense of lateral resolution. In our experiment, the raw data were obtained by a 2.25 MHz nonfocused transducer instead of a focused one, as in traditional LMTT, and the synthetic-aperture reconstruction method based on the delay-and-sum algorithm was applied to reconstruct the images. By applying the synthetic-aperture method, we have improved the lateral resolution of the images and enhanced our ability to image spherical or oblique boundaries in the samples. Images acquired from two microwave sources with different frequencies were compared; the 3 GHz system has a much larger imaging depth but a lower SNR than the 9 GHz system in near-surface imaging.

II. METHODS

A. Reconstruction method

The image reconstruction method is illustrated in Fig. 1. For convenience, we converted both the signal-delay time

 0094-2405/2001/28(12)/2427/5/$18.00

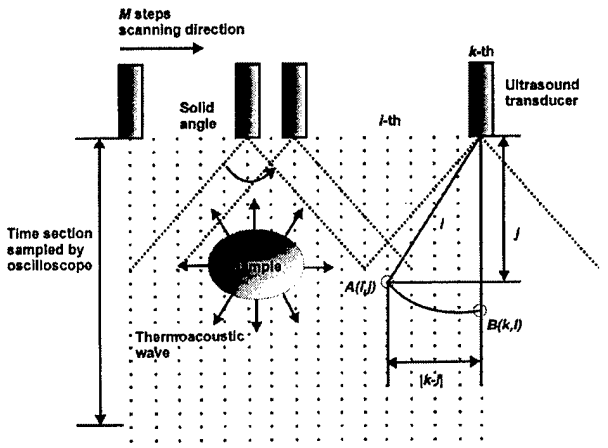

FIG. 1. Scanning and reconstruction method.

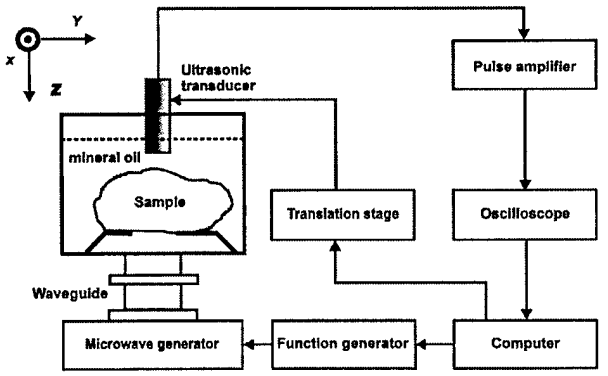

FIG. 2. Experimental setup.

and the spatial distance into the number of pixels according to the speed of the acoustic wave traveling in the media. For the 50 MHz sampling rate, 1 μs= 50 pixels= 1.5 mm.

Because the transducer is nonfocused, it receives signals from a larger solid angle than does a focused counterpart. In the reconstruction, we evenly projected the signals to each point within the whole solid angle according to the time delay. The time delay corresponds to the distance from the transducer to the point to which we project the signal. This is the algorithm called "delay and sum." In other words, the signal intensity of each point $A(i,j)$ is the sum of the signals from the transducer at different positions delayed with the transit time from the transducer position to the point. So the signal intensity at any point, $A(i,j)$, can be expressed as

$$A(i,j)=\sum_{k=0}^{M} B(k,l),$$

where $B(k,l)$ is the signal intensity coming from the lth pixel point in the signals and from the kth transducer scanning position, M is the total number of steps that the transducer scanned, and l is the distance from the kth transducer scanning position to the point (i,j):

$$l=\sqrt{(k-i)^2+j^2}.$$

Let us consider a point (i_1,j_1) where there is a thermoacoustic source. During the data acquisition, all the detectors will receive signals from this particular point after time delays determined by the above equation. Conversely, in the reconstruction, all the detectors contribute signals to this particular point with the appropriate time delays. On the other hand, for a point (i_2,j_2) where there is no source, few detectors contribute signals to this point after time delays determined by the above equation. Consequently, the reconstructed intensity at point (i_1,j_1) will be much greater than that at point (i_2,j_2). In this reconstruction scheme, the detection can be artificially focused onto any specified point (i,j), which is the basic concept of synthetic aperture.

We attempted to add some corrections to the delay-and-sum algorithm but found them unnecessary. For example, we tried applying weights to the signals according to the transducer's directivity, as was done previously. It improved the SNR, but the lateral resolution deteriorated as a result. In our situation, we had already acquired a satisfactory SNR by averaging the thermoacoustic signals 100 to 200 times, indicating that the direct delay-and-sum algorithm works well in LMTT technology.

B. Experimental setup

The experimental setup for this study is shown in Fig. 2. A Cartesian system was set up for reference. The z axis is along the ultrasonic axis pointing downward. The x axis is perpendicular to the drawing plane and pointed outward. The y axis is in the drawing plane and points to the right.

In the experimental setup, microwave pulses of 9 or 3 GHz, with a width of 0.5 μs were delivered into the samples. The sizes of the cross section of waveguides were 72 mm $\times$ 34 mm in the 3 GHz system and 23 mm $\times$ 10 mm in the 9 GHz system. A function generator (DS345, Stanford Research System) was employed to trigger the microwave pulses and synchronize the sampling of an oscilloscope. A linear translation stage (MD2, Arrick Robotics), on which an ultrasonic transducer was mounted, was driven by a computer-controlled stepper motor. The transducer was scanned linearly. The nonfocused ultrasonic transducer (V323, Panametrics) mounted on the translation stage had a central frequency of 2.25 MHz and a 6 mm diam of an active element. A low-noise pulse preamplifier (500 PR, Panametrics) amplified the acoustic signals coming from the transducer. Then the amplified signals were collected and averaged by an oscilloscope (TDS-640A, Tektronix) and subsequently transferred to a personal computer. The acoustic waves from the sample were coupled to the ultrasonic transducer by mineral oil.

III. RESULTS AND DISCUSSION

In this section, we will present and discuss the images acquired from the 3 GHz microwave system and the 9 GHz microwave system, respectively. The first two sets of images were acquired from the 9 GHz system. In the first set of images, we imaged a semicylindrical fat sample with a

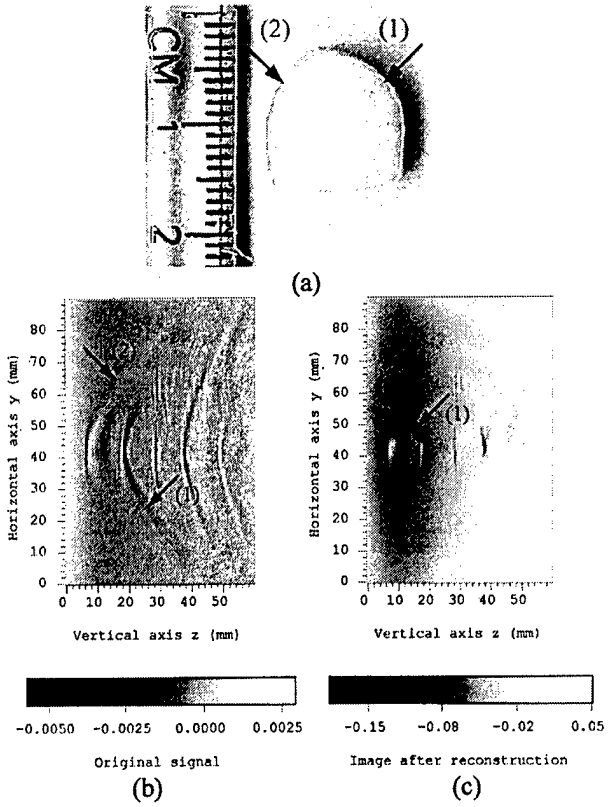

FIG. 3. (a) Cross-sectional picture of the sample with two curved boundaries marked with (1) and (2); (b) raw data of thermoacoustic signals acquired with the 9 GHz system, where the signals from the two curved boundaries are marked with (1) and (2), respectively; (c) image after the reconstruction, where the images of the two curved boundaries are marked with (1) and (2), respectively.

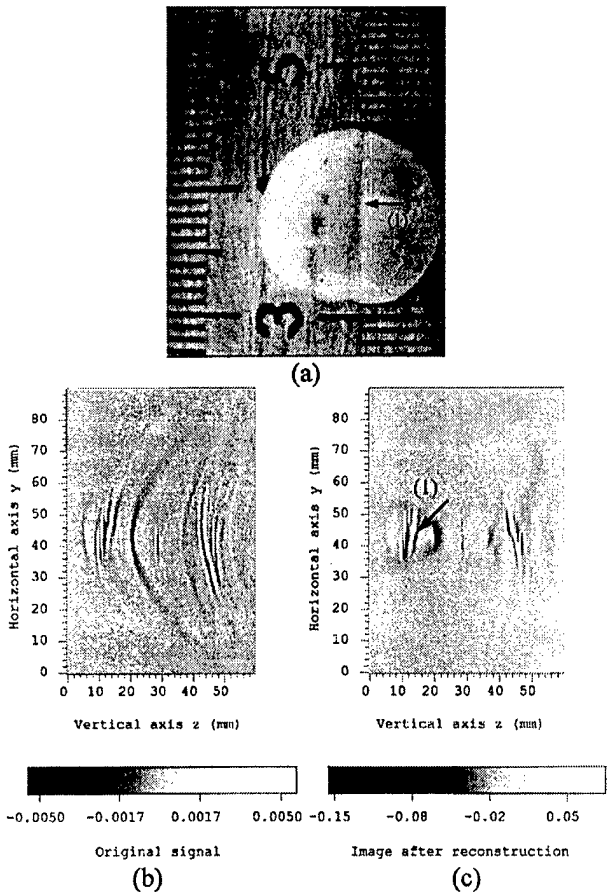

FIG. 4. (a) Cross-sectional picture of the sample, a pork fat cylinder with one layer of connective tissue (1) and discrete layers of muscle; (b) raw data of thermoacoustic signals acquired with the 9 GHz system; (c) Image after the reconstruction, where the images of the connective tissue layer is marked with (1).

simple structure to verify the synthetic-aperture method. In the second set of images, we imaged a small fat cylinder containing several detailed structures. The third set of images was acquired, using the 3 GHz system, from two muscle cylinders buried in an ellipse of pork fat. Comparing the last two sets of images demonstrates the effects of different object shapes and the different frequencies of the microwave sources.

A. Results

The sample in the first set of images is a semicylinder of pork fat immersed in mineral oil. Figure 3(a) shows a cross section of the semicylinder with two curved boundaries marked by (1) and (2). The transducer is on the left side of the picture, pointing to the sample and moving along the ruler. The original signals from the transducer are shown in Fig. 3(b). Because the thermoacoustic waves were propagating almost perpendicularly to the boundaries, the lateral signals (1) and (2) in Fig. 3(b) were from the corresponding curved boundaries (1) and (2) in Fig. 3(a). After reconstruction, the original signals (1) and (2) formed the curved boundaries (1) and (2) of the semicylinder in Fig. 3(c). The synthetic-aperture method was proved to be effective in imaging the curved boundaries. The flat boundary of the semicylinder is not visible in the image because this boundary was parallel to the axis of the transducer. The thermoacoustic waves from this flat boundary traveled perpendicularly to the axis of the transducer and never reached the transducer.

In the second set of images, Fig. 4(a) is the cross section of the sample, which was a pork fat cylinder with one layer of connective tissue (1) and several small pieces of muscle. The transducer was mounted on the left side of the picture, pointing to the sample and moving along the ruler. The images before and after reconstruction are shown in Fig. 4(b) and Fig. 4(c), respectively. The reconstructed image describes the structure of the sample very well. The connective tissue across the cylinder has been imaged clearly, as marked by (1) in Fig. 4(c). The muscles have been imaged as three slides parallel to each other because of the different distances between the muscles and the transducer. Because of the lateral convolution effect caused by the 6 mm diam of the transducer, the images of the muscles were stretched and overlapped along the y direction.

In the 9 GHz system, because of the small cross-sectional area in the 9 GHz waveguide, the microwaves were incident

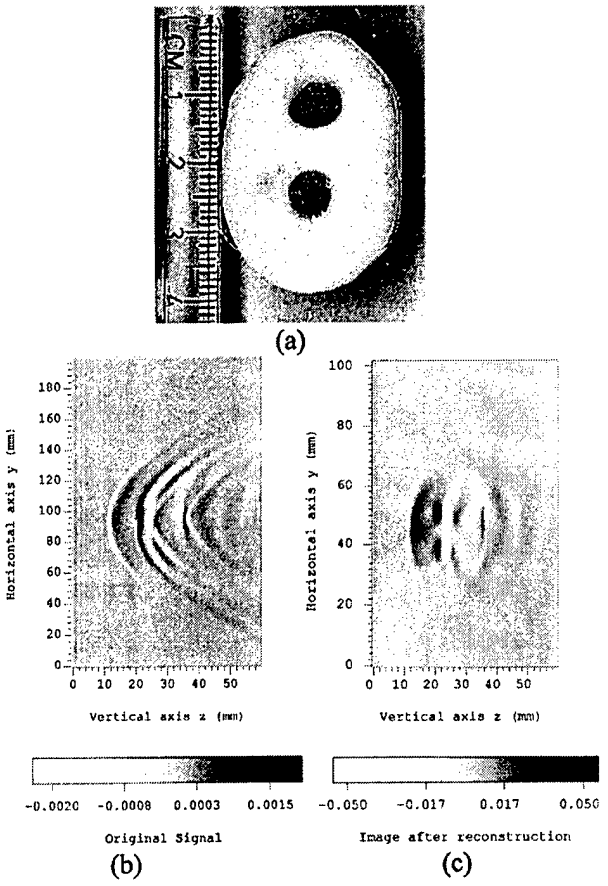

FIG. 5. (a) Cross-sectional picture of the sample, an ellipse of pork fat containing two muscle cylinders; (b) raw data of thermoacoustic signals acquired with the 3 GHz system; (c) image after the reconstruction.

upon the sample from the right to the left side along the transducer axis but in the opposite direction. In this case, the thermoacoustic waves emitted from the left curved edge were smaller than those emitted from the right curved edge. One reason is that the strong microwave absorption of the sample, especially the muscle layers in the sample in Fig. 4, decreased the intensity of the microwave field on the left side. The other reason is that the distribution of the microwave field, without considering sample absorption, also decreased with increasing distance from the sample to the outlet of the waveguide. Therefore, the left boundary of the sample in Fig. 4(c) is much weaker than the right one.

In the above two images acquired with the 9 GHz system, objects in the right part of the image produce a mirror image due to reflected thermoacoustic waves from the boundaries of the container. The reflected signals could be eliminated by time gating, but for comparison they were kept to maintain the same image scale as the images from the 3 GHz system.

The third set of images shown in Fig. 5 was gathered with the 3 GHz system. Shown in Fig. 5(a) is a cross section of the sample, which was an elliptic slab of pork fat with two muscle cylinders buried inside. With the sample being immersed in the mineral oil, the transducer pointed to the sample from the left side and moved along the ruler. In the 3 GHz system, the microwaves were incident upon the sample perpendicularly to the picture and pointed outward, which made the microwaves evenly distributed in the cross section of the sample. In the original signal data in Fig. 5(b), the signals from the muscle cylinder and the edge of the pork fat are spread into a hyperbola with similar shapes. The signals from the two muscle cylinders even cross each other in the center. After the reconstruction, the rebuilt image shown in Fig. 5(c) is in good agreement with the real sample shown in Fig. 5(a).

B. Discussion

From all of the images above, it is clear that the image resolution of curved boundaries of samples and of small cylinders is worse than that of horizontal boundaries, which emit thermoacoustic waves along the transducer axis. For example, the axial resolution of the slabs in Fig. 4(c) is much better than that of the two small cylinders in Fig. 5(c). The reason is that when the thermoacoustic wave does not come from the center of the transducer's receiving solid angle, it may reach different parts of the transducer surface at different times. In this case, the pulse signal is broadened and this broadening of the pulse is proportional to the dimensions of the transducer surface. If the thermoacoustic waves come from the center of the receiving solid angle of the transducer, the resolution is optimized. The propagating direction of most thermoacoustic waves from curved boundaries and small cylinders have large angles with the transducer axis. In other words, when the transducer detects these thermoacoustic waves, they are not from the center of the receiving solid angle. Therefore even after reconstruction, the axial resolution of the curved boundaries or small cylinders has been compromised. Also because of the 6 mm diam of the transducer, all of the images have been stretched along the y direction and the lateral resolution has deteriorated. Therefore, the diameter of the active element of the transducer is a key to both the axial and lateral resolutions. We can alleviate the effect of stretching and improve the axial resolution of the images by reducing the diameter of the transducer at the cost of losing the SNR.

Comparing the above images before and after reconstruction, the SNR has been greatly improved by the reconstruction. In the delay-and-sum algorithm, the signal intensity of every point is the sum of the signals from different positions that the transducer scanned. From the perspective of the SNR and randomization of the noise, summing up signals from k different positions has the equivalent effect of averaging the signal k times and will increase the SNR by $\sqrt{k}$ times. We can take advantage of this property to greatly reduce our average time in data acquisition and the dose of microwaves.

A comparison of the images in Fig. 4(c) and Fig. 5(c) shows that the 3 GHz system has a much larger image volume than the 9 GHz system due to the deeper penetration depth of the microwaves with a lower frequency and a larger cross section of the waveguide. For microwaves of 3 GHz, the penetration depths for muscle and fat are 1.2 and 9 cm,

respectively, and for microwaves of 9 GHz, the penetration depths for muscle and fat are 0.27 and 2.6 cm. The depth we can image in the tissues is proportional to the penetration depth of the microwaves in the tissue. On the other hand, in near-surface imaging the 9 GHz setup has a better SNR than the 3 GHz system due to the larger attenuation of 9 GHz microwaves and the higher-power density of the microwave source.

In traditional LMTT, the ghost caused by the relatively small diameter of the focused transducer affects the lateral resolution. In synthetic aperture, the scanning nonfocused transducer can be artificially focused onto any specified point and the effect equals a focused transducer with a diameter of the scanning dimension. The large diameter, which is much larger than the diameter of the focused transducer used in conventional LMTT, greatly reduces the ghost and, therefore, improves the lateral resolution of the image.

In our study we point out that, compared with traditional LMTT, the synthetic-aperture method is effective for improving the lateral resolution of images and imaging the curved boundaries in samples. The resolution of the images can be further improved by reducing the diameter of the transducer or applying deconvolution with respect to the finite size of the transducer surface.

According to the IEEE standard, our case involves exposures under a controlled environment, which means the exposure is incurred by persons who are aware of the potential of exposure. For both the 3 and 9 GHz microwaves under a controlled environment, the upper limit of safe exposure is 10 mW/cm^2. If it is used for partial body exposure, the upper limit is relaxed to 20 mW/cm^2 for 3 GHz microwaves and 22.1 mW/cm^2 for 9 GHz microwaves. The peak power of our 3 GHz microwave generator is 10 kW; the microwave pulse width is 0.5 μs; the pulse repetition rate is less than 40 Hz; and the outlet of the microwave generator is 72 mm $\times$ 34 mm. As a result, the power density of the 3 GHz microwave system is 8.2 mW/cm^2. The peak power of our 9 GHz microwave generator is 25 kW; the microwave pulse width is 0.5 μs; the pulse repetition rate is about 2 Hz; and the outlet of the microwave generator is 23 mm $\times$ 10 mm. Consequently, the power density of the 9 GHz microwave system is 10.9 mW/cm^2. Further, we assumed that the entire microwave has been coupled out of the waveguide without divergence. In practice, however, only part of the microwave is coupled out of the waveguide and diverged into a much larger area than the outlet of the waveguide. The power densities used in our experiments are below the limits of the IEEE standard and are safe to humans.

IV. CONCLUSIONS

The synthetic aperture, which has never been used in LMTT, is proved to be a powerful image reconstruction method. The reconstruction method based on the delay-and-sum algorithm has been verified to work well in LMTT because of its ability to image curved boundaries in samples, to improve the lateral resolution, and to reduce the noise of the system. The large diameter of the transducer causes resolution deterioration; the diameter can, however, be reduced to improve the resolution at the expense of the SNR. The comparison of the images shows that the 3 GHz system has a larger imaging volume but a poorer SNR than the 9 GHz system in near-surface imaging.

ACKNOWLEDGMENTS

This project was sponsored in part by the U.S. Army Medical Research and Material Command Grant No. DAMD17-00-1-0455, the National Institutes of Health Grants No. R01 CA71980 and No. R21 CA83760, the National Science Foundation Grant No. BES-9734491, and Texas Higher Education Coordinating Board Grant No. ARP 000512-0123-1999.

[a]Author to whom correspondence should be addressed. Telephone: 979-847-9040; fax: 979-845-4450; electronic mail: LWang@tamu.edu; URL: http://oilab.tamu.edu

[1] W. Joines, R. Jirtle, M. Rafal, and D. Schaeffer, "Microwave power absorption differences between normal and malignant tissue," Int. J. Radiat. Oncol., Biol., Phys. **6**, 681–687 (1980).

[2] S. Chaudhary, R. Mishra, A. Swarup, and J. Thomas, "Dielectric properties of normal human breast tissues at radiowave and microwave frequencies," Indian J. Biochem. Biophys. **21**, 76–79 (1984).

[3] W. Joines, Y. Zhang, C. Li, and R. Jirtle, "The measured electrical properties of normal and malignant human tissues from 50–900 MHz," Med. Phys. **21**, 547–550 (1994).

[4] L. E. Larsen and J. H. Jacobi, in *Medical Applications of Microwave Imaging* (IEEE, Piscataway, NJ, 1986).

[5] S. Caorsi, A. Frattoni, G. L. Gragnani, E. Nortino, and M. Pastorino, "Numerical algorithm for dielectric-permittivity microwave imaging of inhomogeneous biological bodies," Med. Biol. Eng. Comput. **29**, NS37–44 (1991).

[6] M. S. Hawley, A. Broquetas, L. Jofre, J. C. Bolomey, and G. Gaboriaud, "Microwave imaging of tissue blood content changes," J. Biomed. Eng. **13**, 197–202 (1991).

[7] P. M. Meaney, K. D. Paulsen, and J. T. Chang, "Near-field microwave imaging of biologically-based materials using a monopole transceiver system," IEEE Trans. Microwave Theory Tech. **46**, 31–45 (1998).

[8] L.-H. V. Wang, X. Zhao, H. Sun, and G. Ku, "Microwave-induced acoustic imaging of biological tissues," Rev. Sci. Instrum. **70**, 3744–3748 (1999).

[9] G. Ku and L.-H. V. Wang, "Scanning thermoacoustic tomography in biological tissue," Med. Phys. **27**, 1195–1202 (2000).

[10] G. Ku and L.-H. V. Wang, "Scanning microwave-induced thermoacoustic tomography: signal, resolution, and contrast," Med. Phys. **28**, 4–10 (2001).

[11] C. G. A. Hoelen, F. F. M. Demul, R. Pongers, and A. Dekker, "Three-dimensional photoacoustic imaging of blood vessels in tissue," Opt. Lett. **23**, 648–650 (1998).

[12] C. G. A. Hoelen, R. Pongers, G. Hamhuis, F. F. M. Demul, and J. Greve, "Photoacoustic blood cell detection and imaging of blood vessels in phantom tissue," SPIE **3196**, 142–153 (1998).

[13] A. A. Karabutov, E. V. Savateeva, N. B. Podymova, and A. A. Oraevsky, "Backward mode detection of laser-induced wide-band ultrasonic transients with optoacoustic transducer," J. Appl. Phys. **87**, 2003–2014 (2000).

[14] R. A. Kruger, P. Liu, Y. R. Fang, and C. R. Appledorn, "Photoacoustic ultrasound (PAUS)—Reconstruction tomography," Med. Phys. **22**, 1605–1609 (1995).

High-resolution thermoacoustic tomography of biological tissue

Minghua Xu, Xueding Wang and Lihong V. Wang*
Optical Imaging Laboratory, Biomedical Engineering Program,
Texas A&M University, 3120 TAMU, College Station, Texas 77843-3120

ABSTRACT

A study of pulsed-microwave-induced thermoacoustic tomography in biological tissues is presented. A backprojection algorithm based on rigorous theory is used to reconstruct the cross-sectional image from the thermoacoustic measurement in a circular configuration that encloses the sample under study. The results demonstrate the possibility of application in detecting small tumors buried in biological tissues using microwave absorption contrast and ultrasound spatial resolution. Finally, the method is compared with laser-induced thermoacoustic tomography.
Keywords: Thermoacoustic imaging, Tomography

1. INTRODUCTION

Pulsed microwave-induced thermoacoustic tomography combines the advantages of both ultrasound spatial resolution and microwave absorption contrast [1]–[4]. With this technique, a very short microwave pulse (<1 microsecond) heats a sample; the sample then absorbs the microwave energy in a confined time and simultaneously generates temporal thermoacoustic waves, which are strongly related to the locally absorbed microwave energy. The thermoacoustic signals have a wide frequency range up to ~ MHz and carry the information about microwave absorption distribution with millimeter spatial resolution. In practice, microwaves at 300 MHz ~ 3 GHz with 0.1 ~ 1 μs pulse are often adopted, which provide several centimeters penetration depths in biological tissues. Due to the bounded water and salt that exist in cancer cells, a tumor absorbs more microwave energy and generates more intense thermoacoustic waves than the surrounding tissues [5], [6]. The wide range of absorption values among various tissues makes it possible to achieve a high image contrast. In addition, the long penetration depth allows this technique to detect interior tumors.

In this paper, we present our study of pulsed-microwave-induced thermoacoustic tomography under a circular measurement configuration in biological tissues. A wide beam of short-pulse microwave energy is used to illuminate a sample from the bottom. An unfocused ultrasonic transducer with a small aperture is used to record the thermoacoustic signals. A backprojection method based on rigorous theory is used to reconstruct the cross-sectional image from the measured data. A phantom sample is investigated. The reconstructed image agrees with the original sample very well. Finally, the method is compared with laser-induced thermoacoustic tomography.

2. METHOD

A schematic view of the circular measurement system for our study is shown in Fig. 1. A plexiglass container is filled with mineral oil. An unfocused transducer is immersed inside it and fixed on a rotation device. A step motor drives the rotation device and then moves the transducer scan around the sample on a horizontal x-y plane, where the transducer horizontally points to the rotation center. A sample is immersed inside the container and placed on a holder, which is made of thin plastic material that is transparent to the microwave. The transducer (V323, Panametrics) has a central frequency of 2.25 MHz, and a diameter of 6mm. The microwave pulses transmitted from a 3-GHz microwave generator have a pulse energy of 10 mJ and a pulse width of 0.5μs. A function generator (Protek, B-180) is used to trigger the microwave generator, control its pulse repetition frequency, and synchronize the oscilloscope sampling. Microwave energy is delivered to the sample by a rectangular waveguide with a cross section of 72 mm × 34 mm. A personal computer is used to control the step. The signal from the transducer is first amplified through a pulse amplifier, then

* To whom all correspondence should be addressed. Telephone: 979-847-9040; fax: 979-845-4450; electronic mail: LWang@tamu.edu; URL: http://oilab.tamu.edu.

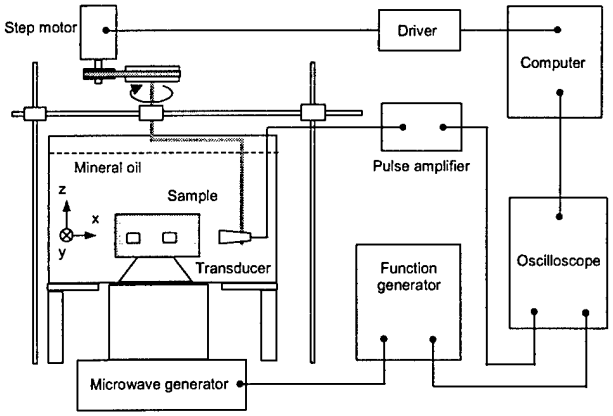

Fig. 1 Schematic of the circular measurement system

recorded and averaged 500 times by an oscilloscope (TDS640A, Tektronix), and finally transferred to a personal computer for imaging.

We assume the tissue to have inhomogeneous microwave absorption and a relatively homogeneous acoustic property. When the microwave pulse duration is < 1 μs, the heat diffusion's effect on the thermoacoustic wave in the tissue can be ignored. The speed of sound c in most soft tissue is relatively constant at ~1.5 mm/μs. Suppose a delta illuminating function $I_0\delta(t)$ and a detected acoustic pressure $p(\mathbf{r}_0,t)$ on the circular surface $\mathbf{r}=\mathbf{r}_0=(\rho_0,\varphi_0,z_0)$ and time t. If challenged to detect small size tumors, we can safely remove the low-frequency component. In addition, the wavelengths of the high-frequency thermoacoustic waves are much smaller than the detecting distances between the thermoacoustic sources and the transducers. Under the above conditions, the spatial absorption function $A(\mathbf{r})$ can be calculated by the following 2D surface integral in the cylindrical configuration

$$A(\rho,\varphi,z)=-\frac{C_p}{2\pi c^4\beta I_0}\int\int_{S_0}\rho_0 d\varphi_0 dz_0\sqrt{1-\frac{(z_0-z)^2}{|\mathbf{r}-\mathbf{r}_0|^2}}\frac{1}{t}\left.\frac{\partial p(\mathbf{r}_0,t)}{\partial t}\right|_{t=\frac{|\mathbf{r}-\mathbf{r}_0|}{c}}, \tag{1}$$

where β is the isobaric volume expansion coefficient and C_p is the heat capacity. The above reconstruction formula indicates that the cross-sectional image of any z plane is determined mainly by the data measured on the circle of the same z plane. In other words, if small absorption sources are located on a z plane, a set of circular measurement data on the same plane can be sufficient to yield a good cross-sectional image.

3. RESULTS AND DISCUSSION

A phantom sample was imaged by our microwave-induced thermoacoustic tomography system. The measurement diagram and its cross-sectional photograph are shown in Fig. 2 (a) and (b), respectively. Three small absorbers, which were made of gelatin, salt and water, were buried inside a large fat base. The transducer rotationally scanned the sample from 0 to 360 degrees with a step size of 2.25 degree. The reconstructed image produced by our backprojection method is shown in Fig. 2 (c), which agrees with the original sample very well. The relative locations and sizes of those thermoacoustic sources perfectly match the buried objects in the original sample.

For comparison, as Fig. 3 shows, an example of two black dots with a gap distance 40 μm was imaged by traditional photoacoustic tomography, in which short laser pulses were used to illuminate the sample. A 10 MHz transducer was used to detect photoacoustic signal. Because the laser duration is only 4.7 ns, a higher frequency thermoacoustic signal was generated and a higher spatial resolution was obtained. However, the laser was not able to penetrate very deeply inside of the tissue.

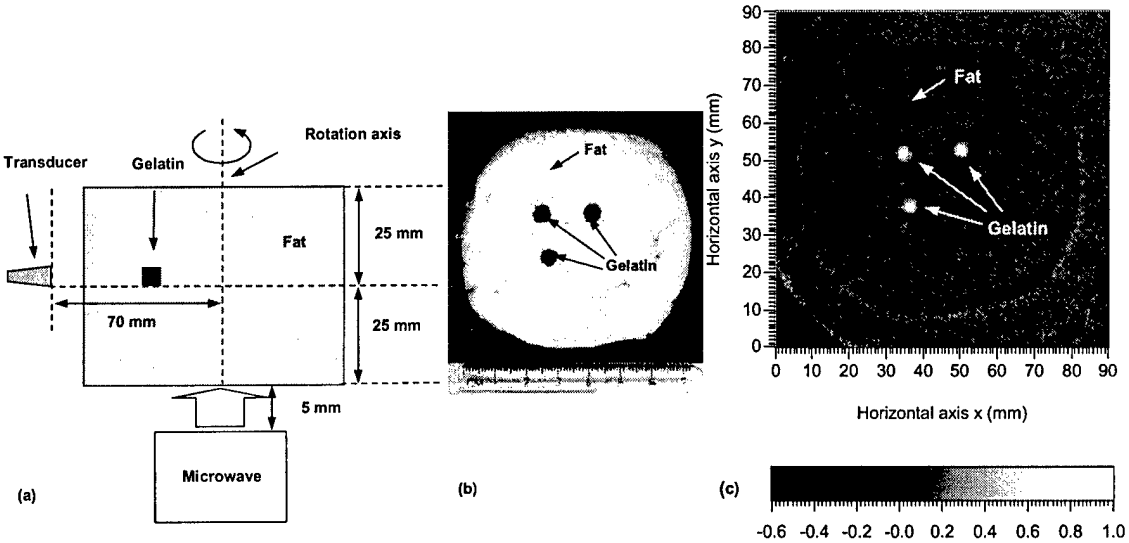

Fig. 2 (a) Diagram of the measurement scheme. (b) Photograph of the sample. (c) Reconstructed image.

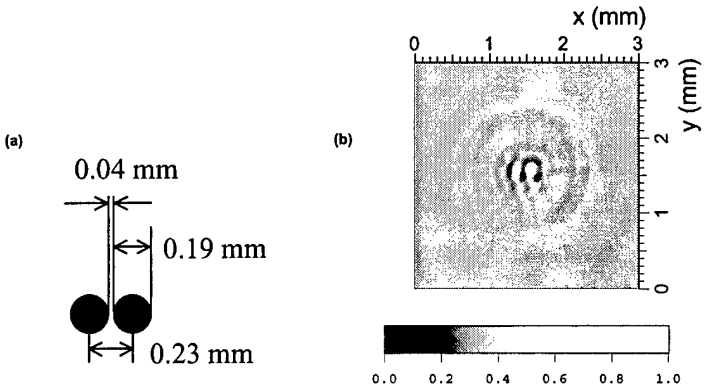

Fig. 3 (a) The schematic of two adjacent dots. (b) The reconstructed image.

4. CONCLUSION

We have presented our study on pulsed-microwave-induced thermoacoustic tomography by a circular measurement configuration in biological tissues. A backprojection algorithm is used to reconstruct the cross-sectional images. The reconstructed image of a phantom sample agrees with the original values very well. The result demonstrates that the circular measurement configuration combined with the backprojection method is a promising technique for use in detecting small tumors buried in biological tissues with microwave absorption contrast and ultrasound spatial resolution (~ mm). Alternatively, a pulsed-laser technique, which provides laser absorption contrast as well as high spatial resolution (~ 50 μm), can be employed as an illumination source to detect small tumors that are not very deeply buried.

ACKNOWLEDGMENTS

This project was sponsored in part by the U.S. Army Medical Research and Materiel Command Grant No. DAMD17-00-1-0455, the National Institutes of Health Grant No. R01 CA71980, the National Science Foudation Grant No. BES-9734491, and Texas Higher Education Coordinating Board Grant No. ARP 000512-0123-1999.

REFERENCES

1. R. A. Kruger, K. K. Kopecky, A. M. Aisen, D. R. Reinecke, G. A. Kruger and W. L. Kiser, "Thermoacoustic CT with radio waves: A medical imaging paradigm," *Radiology* **211**, pp. 275-278, 1999.
2. G. Ku and L.-H. V. Wang, "Scanning thermoacoustic tomography in biological tissues," *Med. Phys.* **27**, pp. 1195-1202, 2000.
3. G. Ku and L.-H. V. Wang, "Scanning microwave-induced thermoacoustic tomography: Signal, resolution, and contrast," *Med. Phys.* **28**, pp. 4-10, 2001.
4. M. H. Xu and G. Ku, and L.-H. V. Wang, "Microwave-induced thermoacoustic tomography using multi-sector scanning", *Med. Phys.* **29**, pp. 1958-1963, 2001.
5. S. Chaudhary, R. Mishra, A. Swarup, and J. Thomas, "Dielectric properties of normal human breast tissues at radiowave and microwave frequencies," *Indian Journal of Biochemistry and Biophysics* **21**, pp. 76–79, 1984.
6. W. Joines, Y. Zhang, C. Li, and R. Jirtle, "The measured electrical properties of normal and malignant human tissues from 50–900 MHz," *Medical Physics* **21**, pp. 547–550, 1994.